Oxazolo[5,4-f]quinoxaline-type selective inhibitors of glycogen synthase kinase-3α (GSK-3α): Development and impact on temozolomide treatment of glioblastoma cells

Mohamed Hasyeoui, Frédéric Lassagne, William Erb, Manal Nael, Khaled Elokely, Apirat Chaikuad, Stefan Knapp, Adrian Jorda, Soraya Vallés, Emie Quissac, et al.

Graphical Abstract

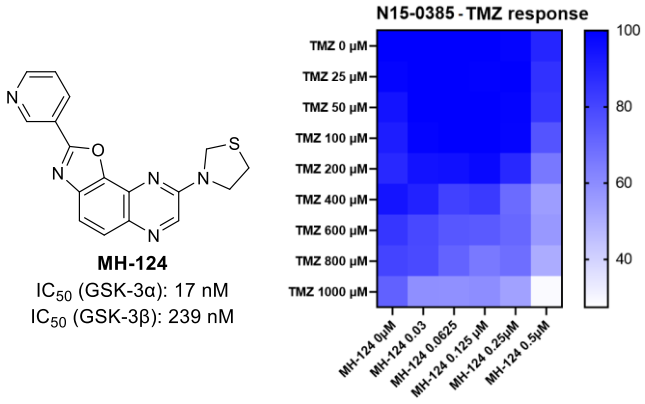

Oxazolo[5,4-*f*]quinoxaline-type selective inhibitors of glycogen synthase kinase-3α (GSK-3α): Development and impact on temozolomide treatment of glioblastoma cells

Mohamed Hasyeoui[a,b], Frédéric Lassagne[a,*], William Erb[a], Manal Nael[c,d], Khaled M. Elokely[d], Apirat Chaikuad[e,f], Stefan Knapp[e,f], Adrian Jorda[g], Soraya L. Vallés[g], Emie Quissac[h], Maïté Verreault[h], Thomas Robert[i,j], Stéphane Bach[i,j,k], Ali Samarat[b], Florence Mongin[a,*]

[a] *Univ Rennes, CNRS, ISCR (Institut des Sciences Chimiques de Rennes) - UMR 6226, F-35000 Rennes, France*

[b] *University of Carthage, Faculty of Sciences of Bizerte, LR18ES11, Laboratory of Hetero-Organic Compounds and Nanostructured Materials, 7021, Bizerte, Tunisia*

[c] *Department of Pharmaceutical Chemistry, Faculty of Pharmacy, Tanta University, Tanta 31527, Egypt*

[d] *Institute for Computational Molecular Science, and Department of Chemistry, Temple University, Philadelphia, PA 19122, USA*

[e] *Institut für Pharmazeutische Chemie, Goethe-Universität Frankfurt, Max-von-Laue-Str. 9, 60438 Frankfurt am Main, Germany*

[f] *Structural Genomics Consortium, Goethe-Universität Frankfurt, Buchmann Institute for Molecular Life Sciences, Max-von-Laue-Str. 15, 60438 Frankfurt am Main, Germany*

[g] *Department of Physiology, School of Medicine, University of Valencia, Blasco Ibañez 15, 46010, Valencia, Spain*

[h] *Sorbonne Université, Institut du Cerveau - Paris Brain Institute - ICM, Inserm, CNRS, APHP, Hôpital de la Pitié Salpêtrière, Paris, France*

[i] *Sorbonne Université, CNRS, UMR8227, Integrative Biology of Marine Models Laboratory (LBI2M), Station Biologique de Roscoff, 29680 Roscoff, France*

[j] *Sorbonne Université, CNRS, FR2424, Plateforme de criblage KISSf (Kinase Inhibitor Specialized Screening facility), Station Biologique de Roscoff, 29680 Roscoff, France*

[k] *Centre of Excellence for Pharmaceutical Sciences, North-West University, Private Bag X6001, Potchefstroom 2520, South Africa*

* Corresponding authors.
E-mail addresses: frederic.lassagne@univ-rennes1.fr (F. Lassagne), florence.mongin@univ-rennes1.fr (F. Mongin).

Keywords: GSK-3α; oxazolo[5,4-*f*]quinoxaline; kinase inhibition; co-crystallization; molecular modelling; glioblastoma

Abstract:

The 2-(3-pyridyl)oxazolo[5,4-*f*]quinoxalines **CD-07** and **FL-291** are ATP-competitive GSK-3 kinase inhibitors. Here, we investigated the impact of **FL-291** on neuroblastoma cell viability and showed that treatment at 10 μM (i.e. ~500 times the IC_{50} against the GSK-3 isoforms) has no significant effect on the viability of NSC-34 motoneuron-like cells. A study performed on primary neurons (non-cancer cells) led to similar results. The structures co-crystallized with GSK-3β revealed similar binding modes for **FL-291** and **CD-07**, with their hinge-oriented planar tricyclic system. Both GSK isoforms show the same orientations for the amino acids at the binding pocket except for Phe130 (α) and Phe67 (β), leading to a larger pocket on the opposite side of the hinge region for the α isoform. Calculations of the thermodynamic properties of the binding pockets highlighted the required features of potential ligands; these should have a hydrophobic core (which could be larger in the case of GSK-3β) surrounded by polar areas (a little more polar in the case of GSK-3α). A library of 27 analogs of **FL-291** and **CD-07** was thus designed and synthesized by taking advantage of this hypothesis. While the introduction of substituents at different positions of the pyridine ring, the replacement of the pyridine by other heterocyclic moieties, or the replacement of the quinoxaline ring by a quinoline moiety did not lead to any improvement, the replacement of the *N*-(thio)morpholino of **FL-291**/**CD-07** by a slightly more polar *N*-thiazolidino led to a significant result. Indeed, the new inhibitor **MH-124** showed clear selectivity for the α isoform, with IC_{50} values of 17 nM and 239 nM on GSK-3α and GSK-3β, respectively. Finally, the efficacy of **MH-124** was evaluated on two glioblastoma cell lines. Although **MH-124** alone did not have a significant impact on cell survival, its addition to temozolomide (TMZ) significantly reduced the TMZ IC_{50} values on the cells tested. The use of the Bliss model allowed a synergy to be evidenced at certain concentrations.

1. Introduction

Since the late 1990s, protein kinases have become popular drug targets since dysregulation of these signaling biomolecules is linked to various diseases [1]. Thus, 71 kinase inhibitors approved by the FDA are already marketed while many other candidates are currently in clinical evaluation [2, 3].

Glycogen synthase kinase-3 (GSK-3) is a family of serine-threonine kinases associated with key biological processes such as metabolism, cell signaling, cell transport, apoptosis, proliferation, and intracellular communication. It is therefore implicated in many diseases such as type 2 diabetes, bipolar disorder, schizophrenia, Alzheimer's and Parkinson's diseases, developmental disorders and cancers, and has therefore become an important target for the development of drugs [4-6].

The Wnt/β-catenin signaling pathway is involved in multiple signaling cascades (Epidermal Growth Factor Receptor, Notch, Nuclear Factor kappa-B, PhosphoInositide 3-Kinase, etc.) and this pathway is therefore important for the initiation and progression of various types of cancer [7]. While the Wnt/β-catenin pathway is dysregulated in some cancers, some treatment strategies have been shown to induce additional pathway activation leading to cancer cells resistance. For example, it has been demonstrated that the PI3K-mediated anti-apoptotic Wnt/β-catenin pathway results in resistance to the alkylating drug temozolomide, which is used to treat glioblastoma (GBM) [8].

Since GSK-3 is a negative regulator of the Wnt/β-catenin and PI3K/Akt pathways, GSK-3 kinases have initially been characterized as growth suppressors. However, many studies have since shown that the inhibition of GSK-3 kinases by small molecules could, on the contrary, lead to antiproliferative activities in many types of cancers. This might be a result of diverse additional roles of both GSK-3 isoforms (α and β) in regulating signaling pathways as well as the limited selectivity of inhibitors used in these studies [9].

Indeed, while the two isoforms of GSK-3, GSK-3α and GSK-3β, have 97% similar amino acid sequences in their catalytic domains and therefore share certain biological functions, the presence of an extended glycine-rich N-terminal region in GSK-3α prevents this isoform from entering the nucleus and renders its biological function and regulation distinct from that of GSK-3β [6]. In particular, GSK-3α

appears to play a specific role in cardiac pathogenesis, atherosclerosis, metabolic disorders (e.g. obesity, insulin resistance and fatty acid accumulation), tissue aging, neurodegenerative disorders, and regulation of solid and hematological malignancies [10].

In the Wnt/β-catenin pathway, GSK-3β mediates the phosphorylation of β-catenin, resulting in its ubiquitination and then degradation by the proteasome. Thus, if GSK-3β were selectively inhibited, the concentration of β-catenin should increase in the cytosol, leading to the migration of unphosphorylated β-catenin into the cell, its accumulation in the cell nucleus, and consequences such as triggering of target genes (e.g. c-Myc), mutations and toxicities [7, 11]. So, while dual GSK-3 inhibitors have already entered clinical trials, none of these inhibitors have passed the early stages of clinical evaluation. It is therefore clinically more relevant to selectively target the α isoform [12, 13].

While most studies have focused on GSK-3β, a few specific inhibitors of GSK-3α are currently under development (Figure 1). Following studies on the development of selective "scorpion-shaped" GSK-3α inhibitors (> 90-fold isoform selectivity for the best inhibitor of this series; with IC_{50} values of 2 nM and 185 nM against GSK-3α and GSK-3β, respectively) [14], Schmidt and co-workers reported the derivative **27** in 2015 (Figure 1a). With an IC_{50} in the nanomolar range for GSK-3α and good aqueous solubility, it has been successfully evaluated in the treatment of acute myeloid leukemia (AML) [15]. In 2018, Wagner et al. designed (racemic) **BRD0705**, a heterocyclic compound that selectively inhibits GSK-3α (8-fold; with IC_{50} of 66 nM and 515 nM against GSK-3α and GSK-3β, respectively; Figure 1b) and capable to arrest the progression of AML without elevation of β-catenin [12]. A year later, Zhang, Liu and co-workers discovered the even more potent inhibitor **G28_14** (7-fold; with IC_{50} of 33 nM and 218 nM against GSK-3α and GSK-3β, respectively; Figure 1c) which also exhibits promising therapeutic properties [16].

In 2020, some of us identified the oxazolo[5,4-*f*]quinoxalines **CD-07** and **FL-291** as potent ATP-competitive GSK-3 kinase inhibitors (Figure 1d) [17]. Since the synthesis of these compounds is straightforward and offers many potential structural modifications, we decided to take advantage of its

promising selectivity towards the α isoform of GSK-3 (5-fold for **CD-07**; with IC_{50} of 4.8 nM and 22 nM against GSK-3α and GSK-3β, respectively) to attempt the development of an even more selective inhibitor. Here we discuss the design of novel analogs of **CD-07** and **FL-291** based on docking studies and report their synthesis and evaluation on kinases.

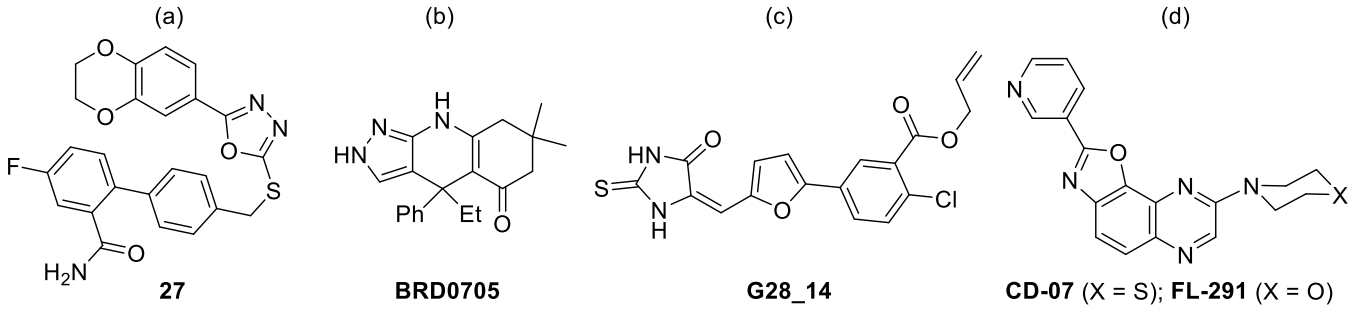

Figure 1. Selective GSK-3α inhibitors previously developed by (a) Schmidt and co-workers [15], (b) Wagner et al. [12], (c) Zhang, Liu and co-workers [16] and Lassagne et al. [17].

Glioblastoma (GBM) is a malignant tumor that represents the most aggressive type of glioma. An important role of GSK-3 in brain cancers such as GBM and neuroblastoma has been identified, however with contrasting results [9]. Considering these data, we also evaluated the activity of our GSK-3α inhibitor on GBM cells.

2. Results and Discussion

2.1. Toxicity study of FL-291 on NSC-34 cells or on neurons in primary culture

Before developing new libraries of **CD-07** and **FL-291** analogs, we were eager to evaluate the toxicity of our hits on neuroblastoma cells. Indeed, the physiology of cholinergic signaling is implicated in numerous neurological functions and pathological changes, including disturbances in Alzheimer's disease (AD) and amyotrophic lateral sclerosis (ALS) [18-20]. However, due to the limited availability of cholinergic motoneurons from spinal cord and lack of culture purity, the NSC-34 cell line has often been used as a model for neurotoxic determination. NSC-34 is a hybrid murine neuroblastoma/spinal

cord cell line produced by fusing mouse neuroblastoma cells with motoneuron-enriched embryonic spinal cord cells [21].

Furthermore, the toxicity of our inhibitor **FL-291** was evaluated on healthy/non-cancer cells (primary neurons taken from cortex fetus of rats) in order to have an idea of the selectivity index likely to be obtained with compounds of this family.

Thus, the effect of **FL-291** on the viability of neuroblastoma cells or neurons in primary culture was first investigated by using MTT (3-(4,5-dimethyl-2-thiazolyl)-2,5-diphenyltetrazolium bromide) conversion assay (reduction of tetrazolium MTT to formazan by metabolically active cells). As shown in Figure 2, incubation of NSC-34 motoneuron-like cells (Figure 2A) or neurons in primary culture (Figure 2B) with high doses of **FL-291** induced a dose-dependent decrease in cell viability. Interestingly, the lowest concentration of **FL-291** used (10 µM), which is already 500 times the IC_{50} against GSK-3 isoforms (Figure 1), has no significant effect on the viability of NSC-34 motoneuron-like cells or in neurons in primary culture.

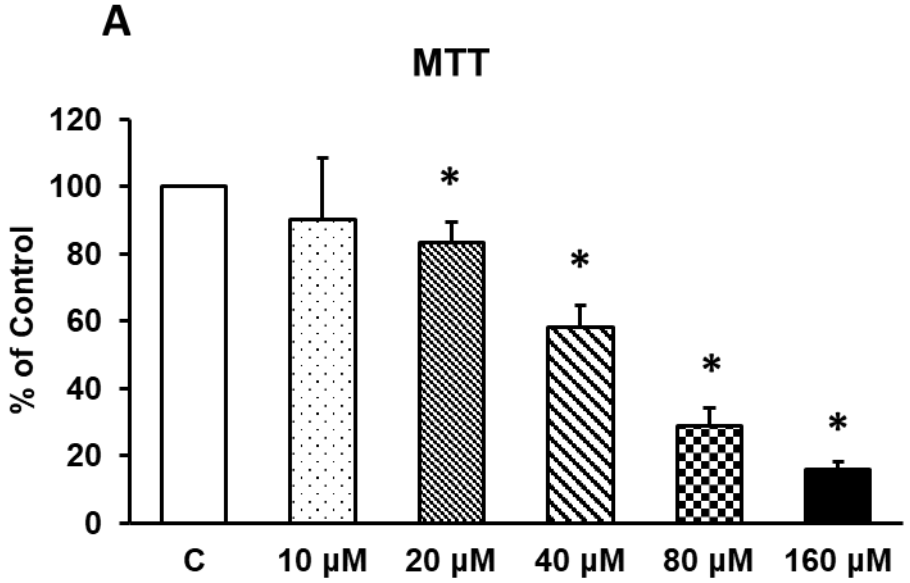

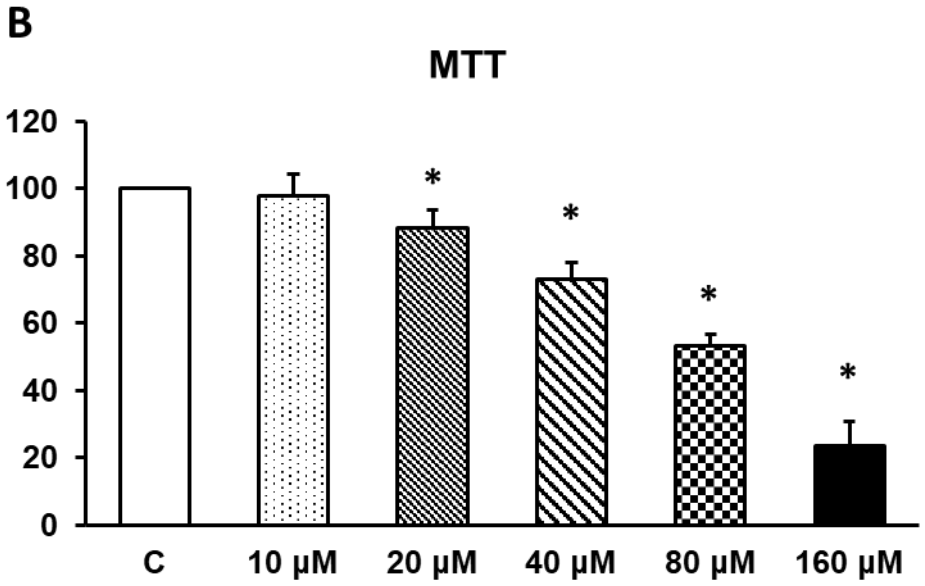

Figure 2. A: Effect of **FL-291** on NSC-34 viability (10 µM, 9.75%; 20 µM, 16.5%; 40 µM, 41.75%; 80 µM, 71.25%; 160 µM, 84.25%). **B**: Effect of **FL-291** on the viability of neurons in primary culture (10 µM, 2.0%; 20 µM, 11.75%; 40 µM, 26.9%; 80 µM, 46.75%; 160 µM, 76.5%). Cell viability was determined by MTT assay in cells treated for 24 h. Cells were incubated without (control, C) or with **FL-291** (10 µM, 20 µM, 40 µM, 80 µM, 160 µM). Data are means ± SD of four independent experiments (each with cells from a different rat). *$p < 0.05$ vs. control.

As the conversion of MTT to formazan can be observed occasionally under conditions where cell death does not occur, we decided to confirm the previous results by using the trypan blue exclusion assay which quantifies the number of viable cells by labeling exclusively dead cells. NSC-34 cells were isolated and seeded at 4 x 10^4 cells/35 mm dish (see Table S1). After 5 days of culture, the cells were incubated without (control, C) or with **FL-291** (20 µM, 40 µM, 80 µM, 160 µM) for 24 h. The data obtained on NSC-34 cells indicate that the decrease observed in Figure 2 correlates with a decrease in the number of live cells (see Supplementary data for details). We did not use a concentration of 10 µM here because no change was detected after adding **FL-291** in the MTT assay.

Confocal microscopy was ultimately used to determine cell death and aggregation within NSC-34. Figure 3 shows that **FL-291** induces cell aggregation and cell death in a concentration-dependent manner. At a concentration of 10 µM, we detected an increase in cell proliferation without cell aggregation compared to control cells, thus demonstrating the protective effects of **FL-291**.

Taken together, these early toxicity assays show that **FL-291** has limited toxicity on NSC-34 cells as well as on neurons in primary culture, and only at a concentration well above the IC_{50} against GSK-3. Therefore, these results confirmed our desire to develop new analogs of **FL-291**.

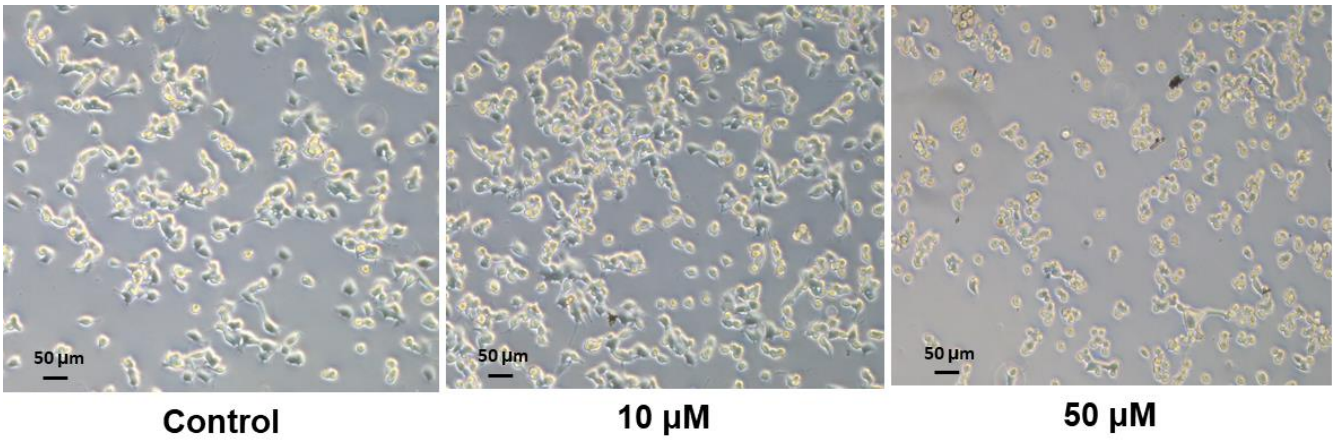

Figure 3. NSC-34 cells monolayers growing on 16-mm glass coverslips were used for viability studies after inhibitor addition. Cell aggregation was determined by confocal microscopy in NSC-34 cells treated for 6 h without or with (10 µM or 50 µM) **FL-291**. Bars represent 50 µm.

2.2. Co-crystallization of FL-291 and CD-07 in GSK-3β and docking studies

To identify the binding modes of **FL-291** and **CD-07**, we determined co-crystal structures of GSK-3β. Both ligands bound to the kinase in a very close conformation and developed similar interactions. The planar tricyclic system was oriented towards the hinge with the quinoxaline moiety forming a hydrogen bond to the hinge Val135 backbone amide nitrogen. The pyridine group protruded into the back pocket and formed another hydrogen bond with the catalytic Lys85. In addition, this pyridine was located close to the Phe67 benzene side chain of the glycine-rich loop which adopted an 'in' conformation. Morpholine from **FL-291** and thiomorpholine from **CD-07** were projected outward to the solvent-exposed channel, but still close to αD Thr138 and Arg141, although too far for direct contact. The morpholine and thiomopholine fragments were also found to have two different ring conformations in the experimental structure (Figure 4A and 4B).

A homology model was prepared for GSK-3α based on the X-ray crystal structure of the highly similar GSK-3β isoform [22]. Furthermore, as the AlphaFold database was recently updated with many accurate

predicted protein structures, we also downloaded GSK-3α for comparison [23, 24]. The two models were essentially identical, particularly within the kinase domain (Figure 4C and 4D) and a sequence comparison is detailed in the Supplementary data of this manuscript. Both GSK-3 isoforms share the same orientations for the amino acids at the binding pocket except for Phe130 (GSK-3α) and Phe67 (GSK-3β). However, differences in sequence between these two closely related isoforms may result in different dynamic properties. Long-range electrostatic interactions may be influenced by aD sequence variations between the two isoforms, in particular by the change R148K (GSK-3β numbering). The thermodynamics properties of the binding pockets were thus computed to facilitate the design of our new inhibitors (Figure 5).

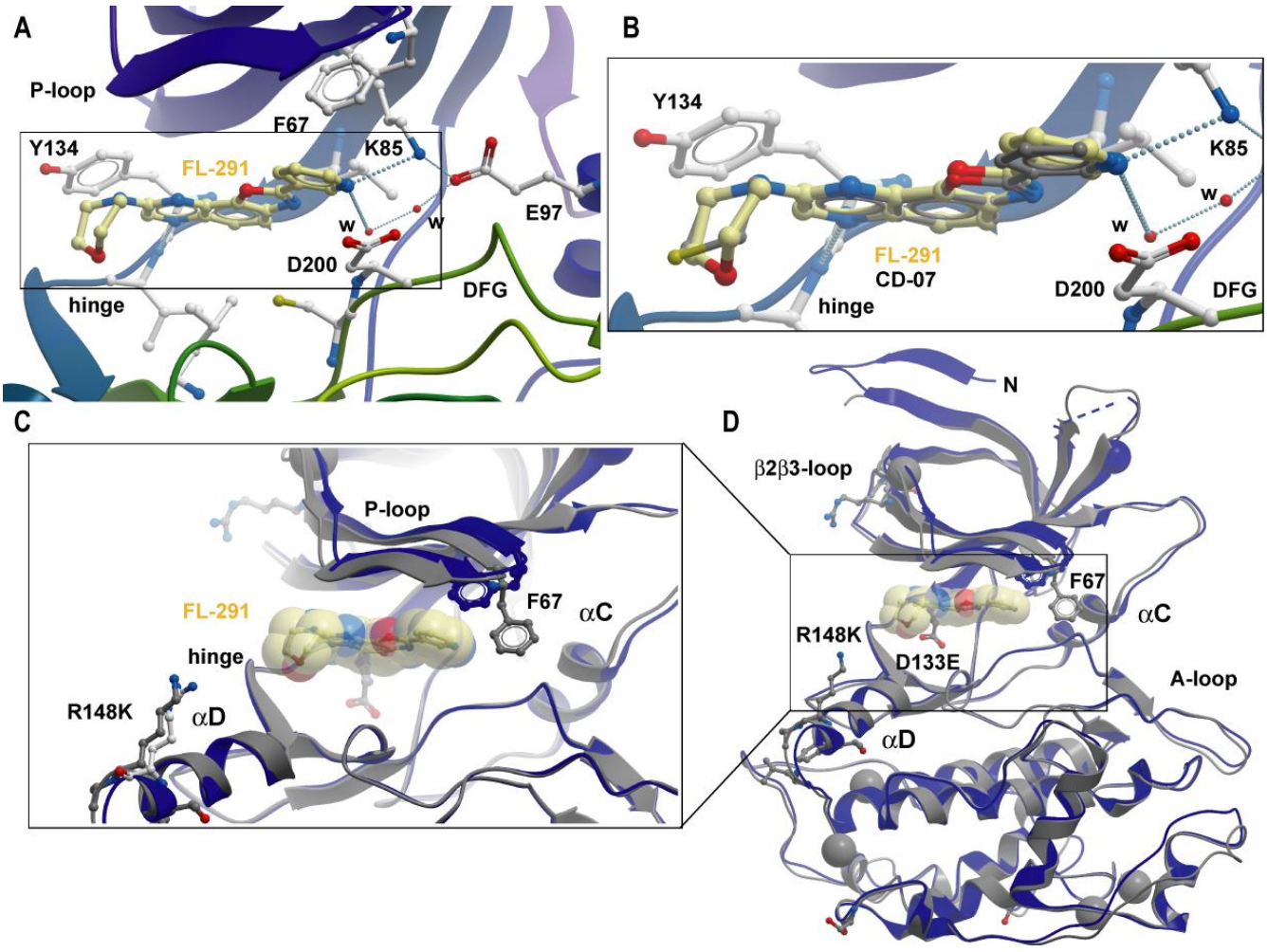

Figure 4. Binding mode of **FL-291** and **CD-07** in GSK-3β and comparison of GSK-3α and GSK-3β. **A**: Binding mode of **FL-291**. The inhibitor is highlighted by yellow carbons in ball and stick representation and the main interacting residues are shown. Hydrogen bonds are shown as dotted lines, including also interactions with water molecules (w). **B**: Superimposition of **FL-291** and **CD-07** (gray

carbon atoms). **C**: Superimposition of the AlphaFold 2 model of GSK-3α and GSK-3β. Shown are structural changes in the ATP binding site. Because the GSK-3α model has been based on the active conformation, the phenylalanine at the tip of the P-loop (F67) in GSK-3β is in a folded conformation in GSK-3β and in the active, outward oriented conformation in the GSK-3α. **D**: Superimposition of the kinase domains of GSK-3α and GSK-3β, showing a high degree of structural conservation. Main differences in primary structures map to the loop region between the β-2 and β-3 sheet as well as to helix αD. Conservative changes are indicated the spheres.

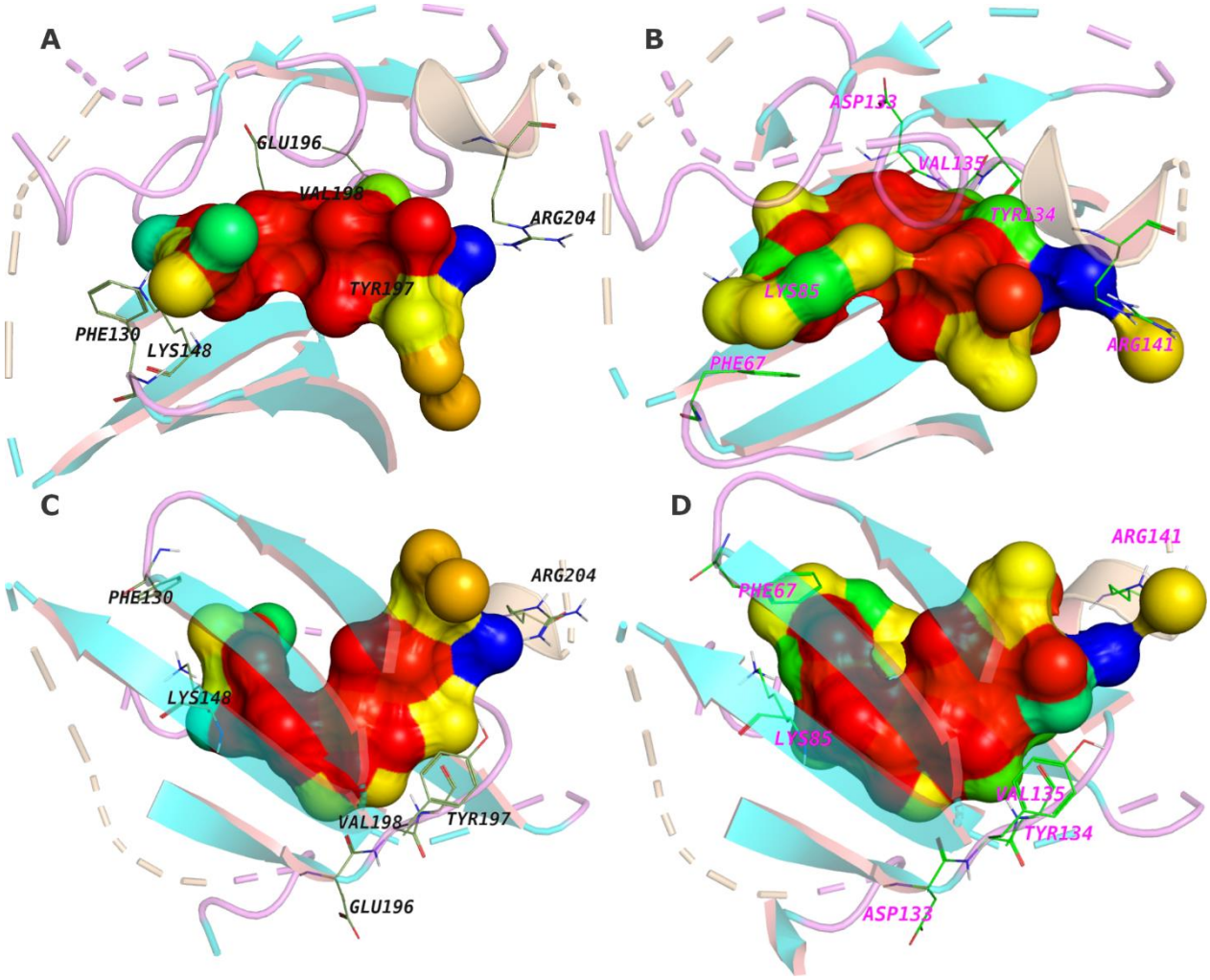

Figure 5. The thermodynamic map of the ligand site at the binding pockets of GSK GSK-3α (**A** and **C**: Top and Side views) and GSK-3β (**B** and **D**: Top and Side view). The surface is colored according to the degree of polarity from red (non-polar) to blue (most polar).

The regions of the thermodynamic maps that represent the features of the ligands (Figures 6-7) are colored according to their electrostatic nature: red for the most non-polar (hydrophobic) regions and yellow (least) to blue (greatest) for polar areas. Thus, the yellow, green, and blue color scheme has been used in the figures to highlight the increased degree of polarity. Based on these data, we hypothesized

that the ligands should possess a hydrophobic core to match the chemical environment of the binding site (Figure 6). Moreover, as shown by the different panels in Figure 5, the hydrophobic core (red central region) could be larger in case of GSK-3β. Around the hydrophobic core, the ligand will need polar groups, as shown by the yellow, green, and blue regions in the thermodynamic maps. In the case of GSK-3α, the ligand features around the central core are slightly more polar (Figure 6). The type and orientation of each substituent can further be guided by water mapping calculations. Indeed, the small spheres around the ligand map (Figure 7) are colored according to the degree of polarity and can serve as a guide for more subtle modifications.

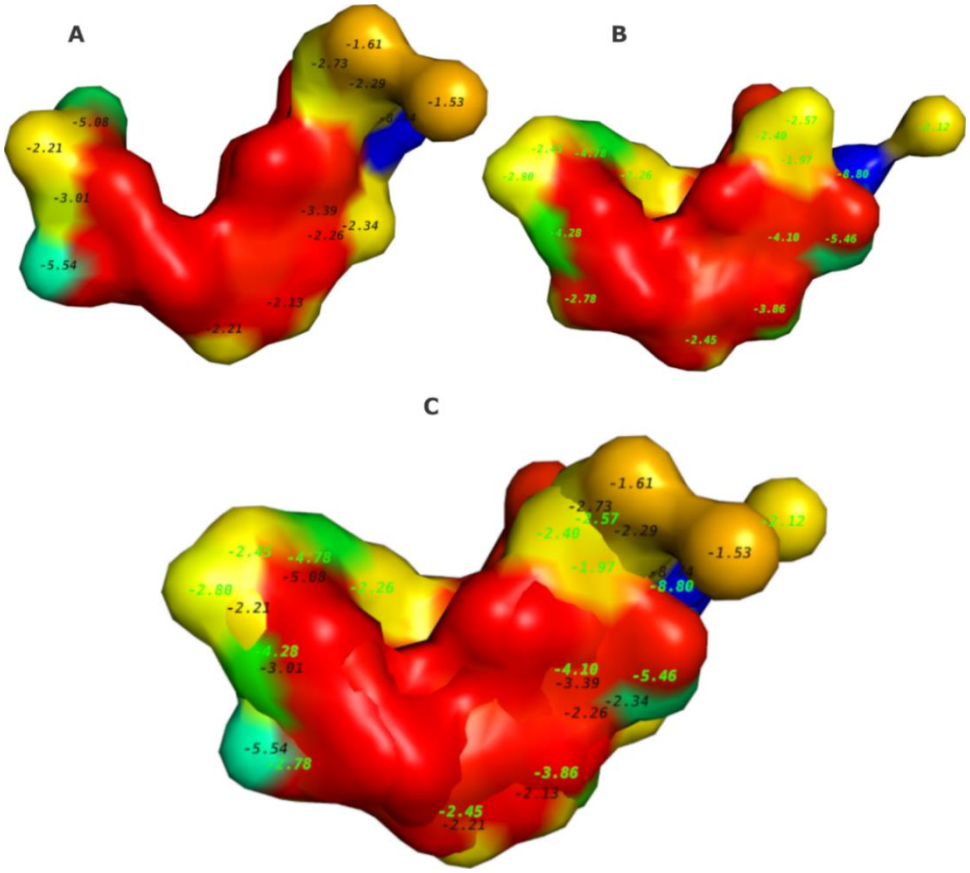

Figure 6. The thermodynamic map of the ligand site of GSK GSK-3α (**A**), GSK-3β (**B**) and aligned surfaces (**C**). The surface is colored according to the degree of polarity from red (non-polar) to blue (most polar). The negative free energy value at each location is shown to define the degree of polarity.

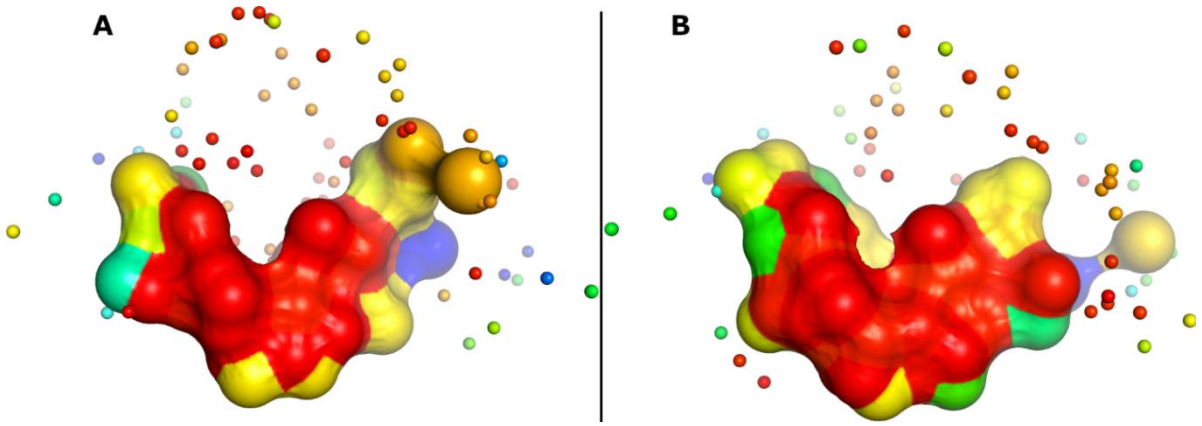

Figure 7. The thermodynamic map of the ligand site of GSK GSK-3α (**A**), GSK-3β (**B**). The surface and the surrounding spheres are colored according to the degree of polarity from red (non-polar) to blue (most polar).

Thus, while keeping in mind the importance of having a simple synthetic route, we determined modifications likely to deliver compounds capable of better interacting with the ATP binding site of GSK-3α. In particular, since the 3-pyridyl group of **CD-07** is close to the larger sub-pocket opposite the hinge region of the α isoform, we decided to introduce various substituents at different positions (R^2, R^4, R^5 and R^6) of the pyridine ring (Figure 8a). We also planned to replace this pyridine with other heterocycles (Figure 8b). Moreover, since the position of **CD-07** in GSK-3α at residues Val198, Tyr197 and Arg204 is slightly different from that in GSK-3β at the corresponding residues Val135, Tyr134 and Arg141, we sought to take advantage of this. We were therefore eager to evaluate the impact of the replacement of the quinoxaline by a quinoline (Figure 8c), as well as the replacement of the thiomorpholine on the interactions developed (Figure 8d).

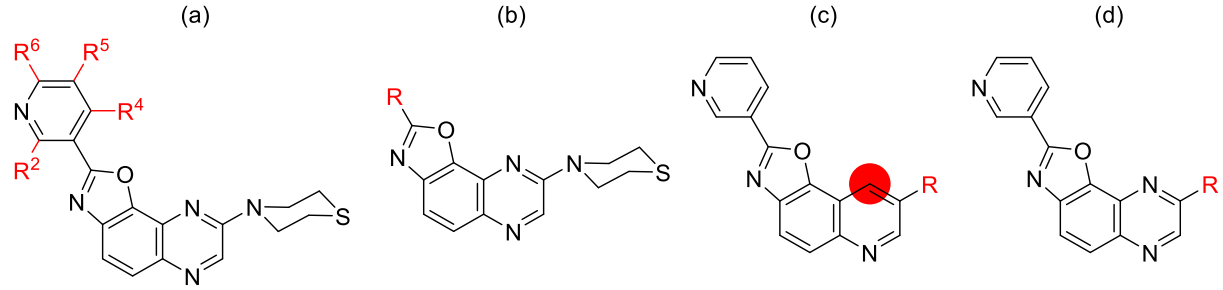

Figure 8. Planned changes from our reference GSK-3α inhibitor **CD-07**.

2.3. Synthesis

In order to access the first set of **CD-07** analogs with different substituents on the 3-pyridyl ring (Figure 8a), we started from 3-chloro-5-iodo-6-quinoxalinamine (**1**) [17] and substituted the chlorine atom using thiomorpholine as a nucleophile in tetrahydrofuran (THF) at reflux in the presence of triethylamine. The obtained product **2** was then reacted [17, 25] with the required substituted nicotinoyl chlorides at room temperature (rt) to provide the carboxamides **3** in good yields. These carboxamides **3** were eventually engaged in a copper-catalyzed cyclizing coupling step in dimethylsulfoxide (DMSO) [17]. The corresponding oxazolo[5,4-*f*]quinoxaline targets **4** were thus obtained with, at the pyridine ring, different substituents, namely Me, OMe or Cl at the 2-position, iPr or CF_3 at the 4-position, Me, F or Br at the 5-position, or Cl at the 6-position (Table 1).

Table 1. Synthesis of the pyridyl-substituted oxazolo[5,4-*f*]quinoxalines **4-2Me**, **4-2OMe**, **4-2Cl**, **4-4iPr**, **4-4CF$_3$**, **4-5Me**, **4-5F**, **4-5Br** and **4-6Cl**.

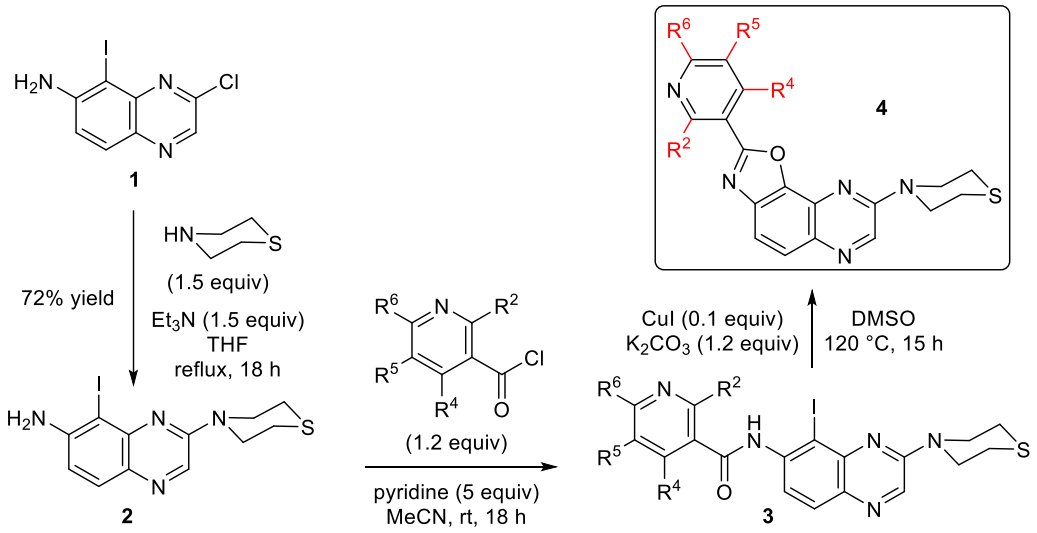

Entry	R^2	R^4	R^5	R^6	**3**, Yield (%)[a]	**4**, Yield (%)[a]
1	Me	H	H	H	**3-2Me**, 76	**4-2Me**, 33
2	OMe	H	H	H	**3-2OMe**, 80	**4-2OMe**, 42
3	Cl	H	H	H	**3-2Cl**, 85	**4-2Cl**, 41
4	H	iPr	H	H	**3-4iPr**, 85	**4-4iPr**, 50
5	H	CF_3	H	H	**3-4CF$_3$**, 78	**4-4CF$_3$**, 78
6	H	H	Me	H	**3-5Me**, 86	**4-5Me**, 68
7	H	H	F	H	**3-5F**, 64	**4-5F**, 67
8	H	H	Br	H	**3-5Br**, 87	**4-5Br**, 47
9	H	H	H	Cl	**3-6Cl**, 89	**4-6Cl**, 74

[a] Yield after purification (see experimental part).

From the carboxamide **3-2Cl** that bears a chlorine atom as a leaving group next to nitrogen of the pyridine ring, nucleophilic substitution using either pyrrolidine or dimethylamine followed by cyclization led to the expected oxazolo[5,4-*f*]quinoxalines **4-2pyrro** and **4-2NMe2**, respectively (Scheme 1a). Another analog, featuring a dimethylamino substituent at the 6-position (**4-6NMe2**) was similarly prepared from **3-6Cl** in two steps (the second step at 110 °C instead of 130 °C, due to its lower steric hindrance; Scheme 1b).

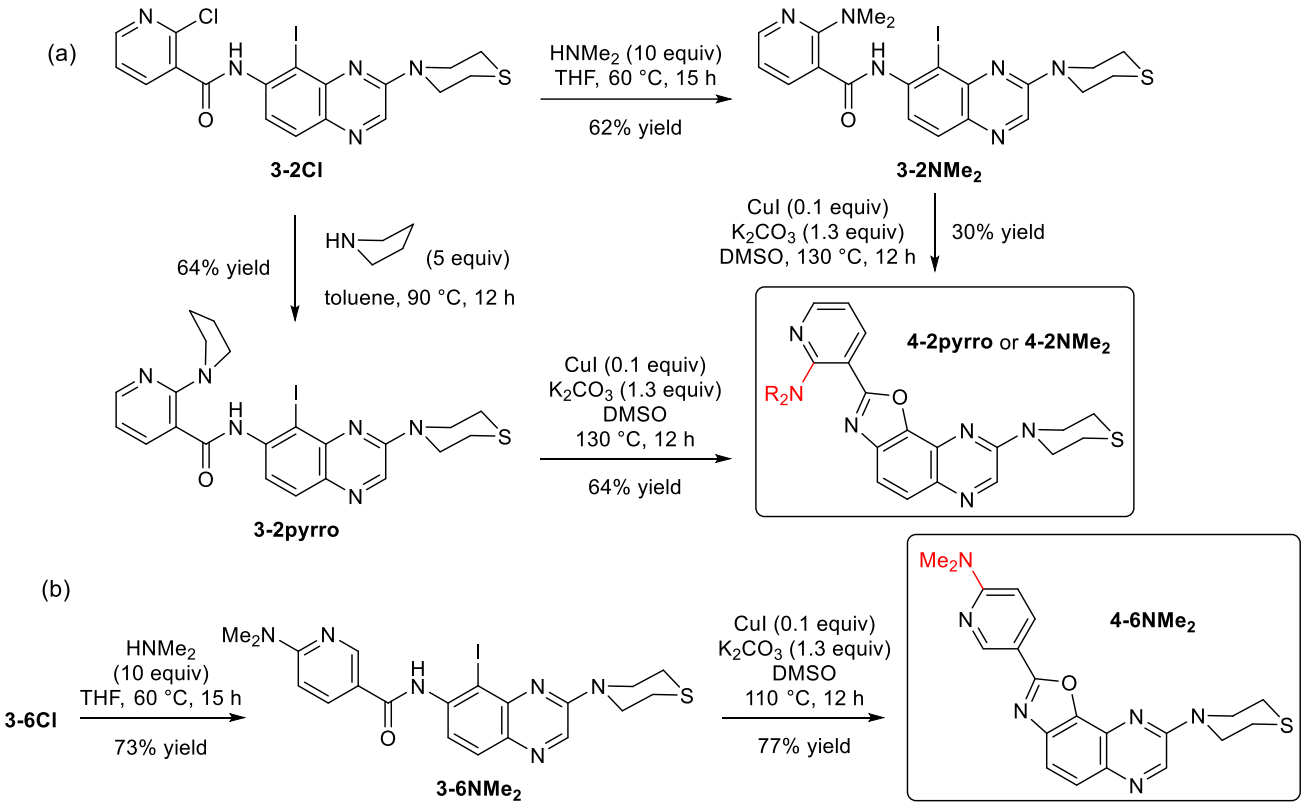

Scheme 1. Synthesis of the pyridyl-substituted oxazolo[5,4-*f*]quinoxalines **4-2pyrro**, **4-2NMe2** (a) and **4-6NMe2** (b).

To reach **4-2F**, the fluorinated isomer of **4-2Cl** (Table 1, entry 3), it was found possible to replace the chlorine atom with a fluorine by treatment with the adduct tetramethylammonium fluoride·(*tert*-amyl alcohol)$_{1.33}$ in DMSO at 80 °C [26] (Scheme 2a). From the tricycle **4-5Br** bearing a bromine atom on the pyridine ring, a Suzuki-Miyaura cross-coupling [27] with thiophene-3-boronic acid led [28] to the oxazolo[5,4-*f*]quinoxaline **4-5thienyl** in good yield, while a palladium-catalyzed Buchwald-Hartwig amination with morpholine [29] resulted in the product **4-5Smorpho** (Scheme 2b). Additionally, the

quinoxaline derivative **4-6Me** was conveniently prepared by Suzuki-Miyaura cross-coupling between the 6-chloro-3-pyridyl-substituted oxazolo[5,4-*f*]quinoxaline **4-6-Cl** and methylboronic acid, according to a protocol inspired by previous operating conditions [30]. Finally, to introduce a two-carbon chain at the 6-position of the pyridine ring, a Sonogashira coupling [31] was carried out between **4-6-Cl** and trimethylsilylacetylene under reported conditions [32]. Subsequent desilylation, by treatment of **4-6CCSiMe3** with catalytic tetrabutylammonium fluoride at room temperature, provided the expected **4-6ethynyl** in 40% overall yield from **4-6Cl** (Scheme 2c).

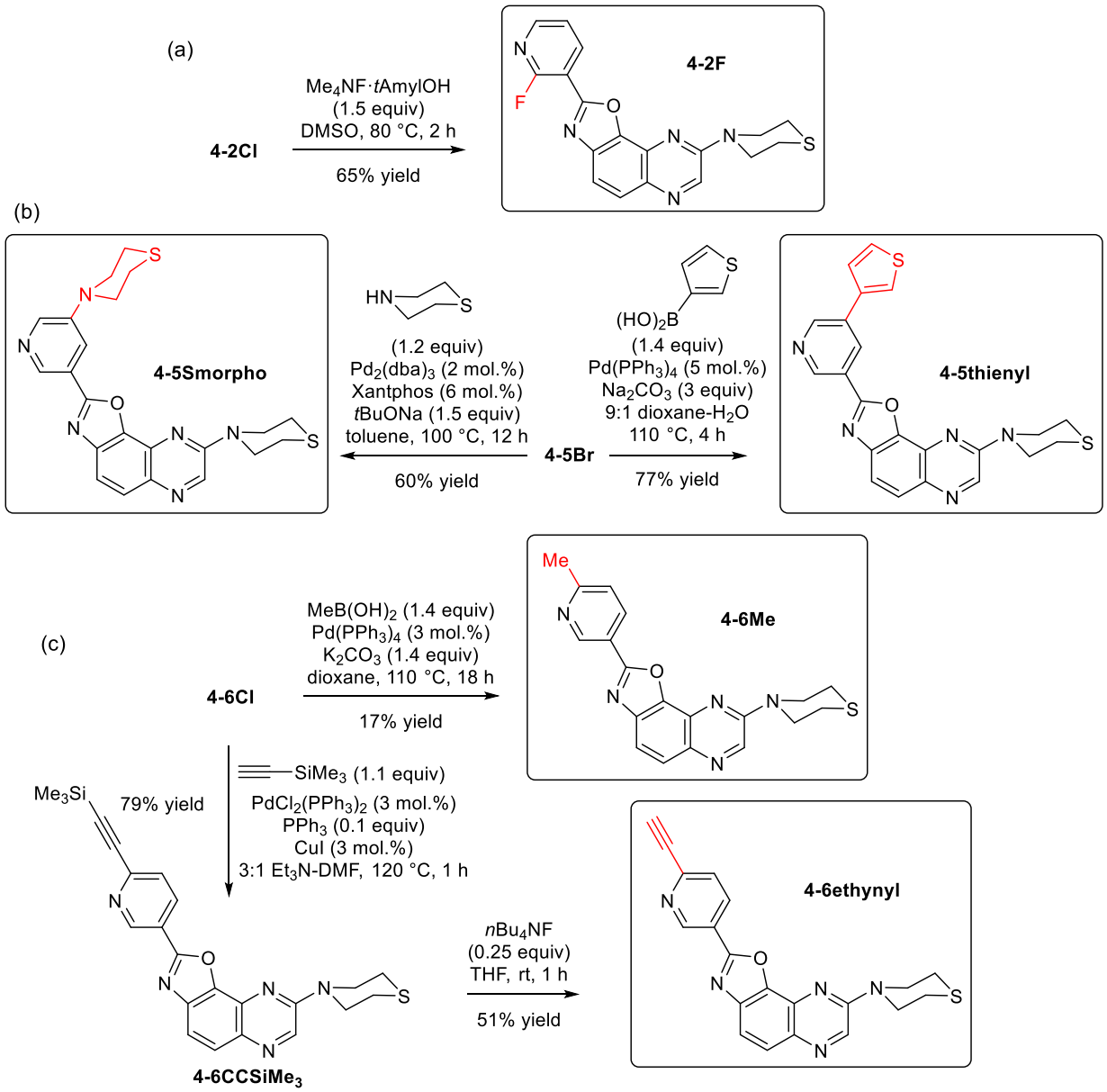

Scheme 2. Synthesis of the pyridyl-substituted oxazolo[5,4-*f*]quinoxalines **4-2F**, **4-5thienyl**, **4-5Smorpho**, **4-6Me** and **4-6ethynyl**.

We then decided to replace the pyridine ring of **CD-07** with other aromatic heterocycles, always keeping one nitrogen oriented toward Lys85 (Figure 8b). For this purpose, we reacted the amine **2** with appropriate aroyl chlorides (or 4-isoquinolinecarboxylic acid, adapting a reported procedure [33], in the case of **5-isoquino**) before carrying out the cyclizing coupling as before. In this way, the oxazolo[5,4-*f*]quinoxalines substituted with 3-quinolyl, 4-isoquinolyl, 1-methyl-4-pyrazyl, 5-thiazyl and 5-isothiazyl groups were obtained with moderate to good yields (Scheme 3).

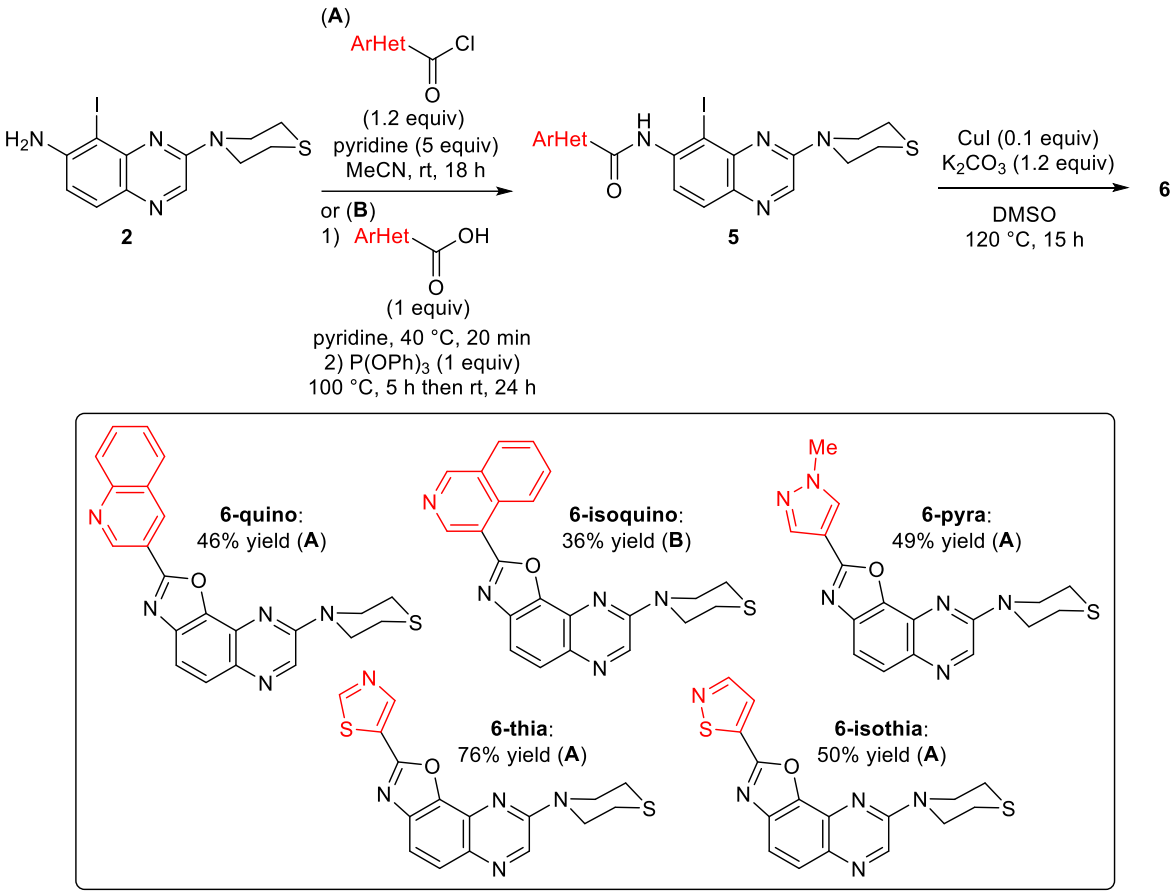

Scheme 3. Synthesis of the heteroaryl-substituted oxazolo[5,4-*f*]quinoxalines **6**, and global yields from **2**.

Our next goal was to replace the quinoxaline core of **CD-07** with a quinoline (Figure 8c). To achieve this objective, we planned to prepare 2-(3-pyridyl)oxazolo[5,4-*f*]quinoline from which a selective bromination at C8 [34] could allow the required thiomorpholino group to be further introduced by a Buchwald-Hartwig amination (Scheme 4a). To validate this approach, we first reacted 3-bromoquinoline

and morpholine under the reaction conditions developed by Kozikowski and co-workers [29] and isolated the coupled product in 81% yield (Scheme 4b).

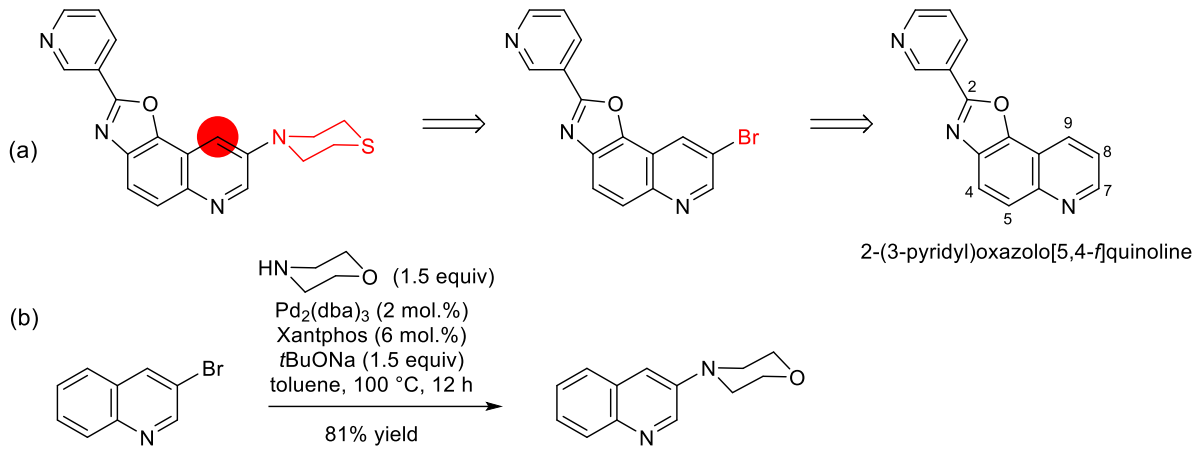

Scheme 4. (a) Retrosynthesis plan to access the quinoline analog of **CD-07** and (b) preliminary results.

To undertake the synthesis of the quinoline analog of **CD-07**, we then started from 6-quinolinamine (**7**) and carried out, as planned [25], its selective iodination at its 5-position. It was then easy to prepare the carboxamide **9** and the oxazoloquinoline **10-H** by using the same conditions as above. In parallel, we also synthesized **14-H** which is the quinoxaline analog of **10-H** (Scheme 5).

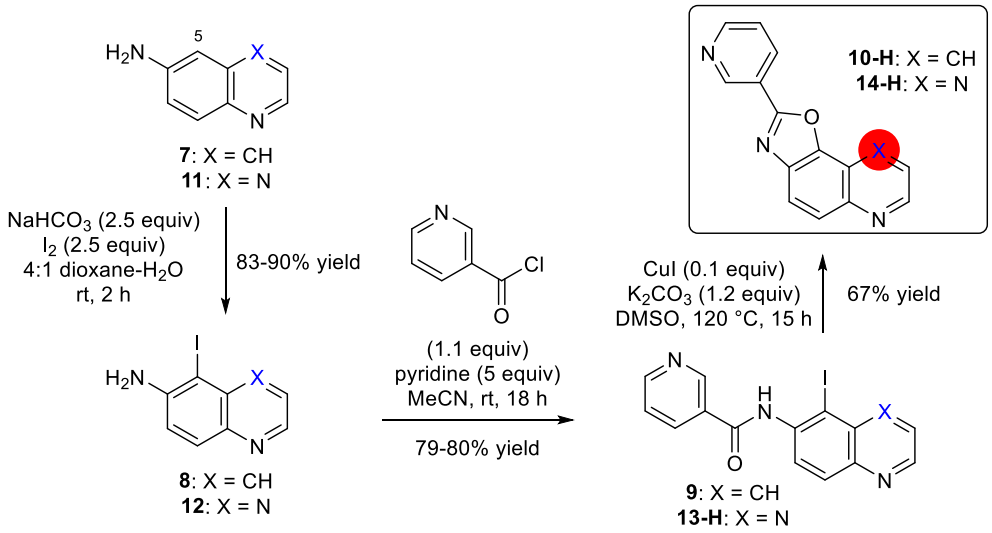

Scheme 5. Synthesis of the quinoline analog of **CD-07** and of 2-(3-pyridyl)oxazolo[5,4-*f*]quinoxaline (**14-H**).

As already observed from substituted quinolines [35], bromination of 2-(3-pyridyl)oxazolo[5,4-*f*]quinoline (**10-H**) proceeded in a fairly regioselective manner to give **10-Br** in 41% yield. Likely due to lower solubility of **10-Br** in toluene compared to 3-bromoquinoline (Scheme 4b), the palladium-catalyzed amination with thiomorpholine worked less efficiently; the expected product **10-Smorpho** was however isolated in 35% yield (Scheme 6).

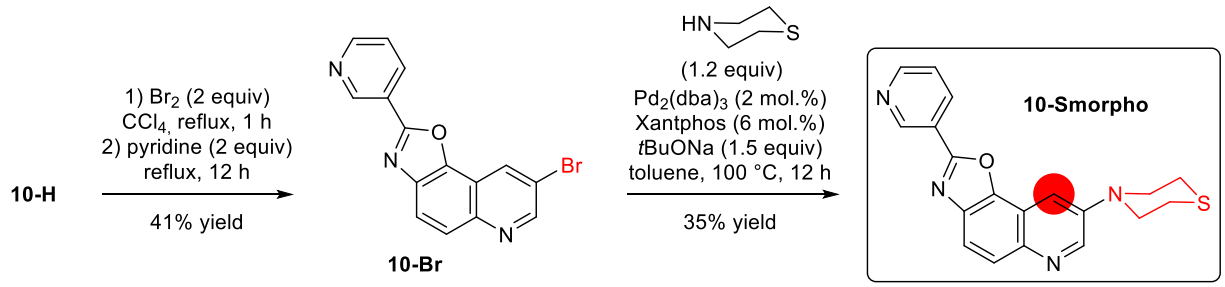

Scheme 6. Synthesis of **10-Smorpho**, the quinoline analog of **CD-07**.

Our end goal was to replace the thiomorpholino group of **CD-07**, which is oriented toward the solvent-exposed region (Figure 8d). The most efficient way to do this would rely on the late-stage functionalization of a common precursor, such as the derivative **14-Cl** in which the chlorine atom could be replaced by direct aromatic nucleophilic substitution or by a metal-catalyzed reaction. As a proof of concept, **14-Cl** was first prepared from 3-chloro-5-iodo-6-(3-pyridoylamino)quinoxaline (**13-Cl**) [17] using a cyclizing coupling procedure slightly modified due to the sensitivity of this compound to nucleophilic attack (Scheme 7, left). Although in moderate yield, chlorine substitution of 8-chloro-2-(3-pyridyl)oxazolo[5,4-*f*]quinoxaline (**14-Cl**) provided the expected derivative **14-thiazo** after treatment with an excess of thiazolidine in the presence of Hünig's base in DMSO at 110 °C (Scheme 7, right).

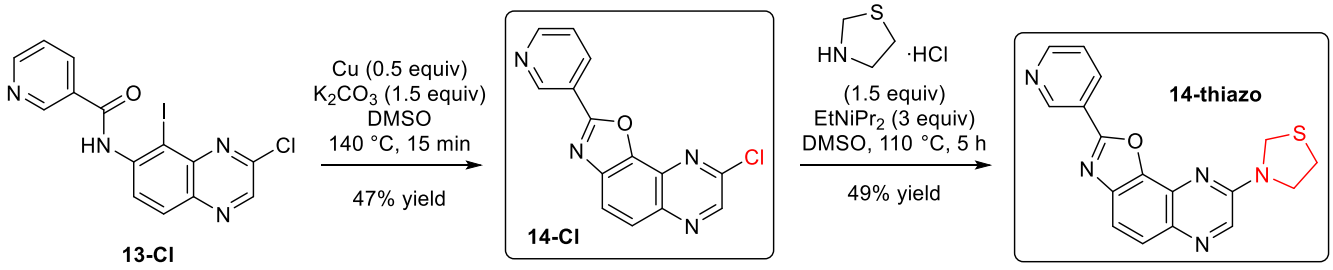

Scheme 7. Synthesis 8-chloro-2-(3-pyridyl)oxazolo[5,4-*f*]quinoxaline (**14-Cl**) and 2-(3-pyridyl)-8-(*N*-thiazolidino)oxazolo[5,4-*f*]quinoxaline (**14-thiazo**).

2.4. Evaluation on kinases and molecular modeling experiments

First, most of the synthesized compounds were evaluated [36] against a panel of eight cancer-related protein kinases: cyclin-dependent kinase 9 (CDK9/Cyclin T), proto-oncogene kinase PIM1, dual specificity tyrosine phosphorylation regulated kinase 1A (DYRK1A), glycogen-synthase kinase-3 (GSK-3 isoforms α/β), casein kinase 1 (CK1 isoform ε), mitotic kinase Haspin and vascular endothelial growth factor receptor 2 tyrosine-protein kinase VEGFR2. Then, IC_{50} values were determined for the most promising inhibitors. The results, presented in Table 2, show that the modifications of the pyridine part (whether it is the introduction of different substituents on the pyridine or the replacement of the latter by other aromatic heterocycles) lead to a loss of affinity for GSK-3 and selectivity for the α isoform. The same is true for the replacement of the quinoxaline core by a quinoline. By far the most promising result concerns **14-thiazo** (or **MH-124**) for which a clear selectivity for the α isoform was observed, with IC_{50} values of 17 nM and 239 nM determined on GSK-3α and GSK-3β, respectively.

However, 2-(3-pyridyl)-8-(*N*-thiazolidino)oxazolo[5,4-*f*]quinoxaline (**14-thiazo or MH-124**) was also found to be a sub-micromolar inhibitor of DYRK1A (IC_{50} value of 68 nM). As DYRK1A and Cdc2-like kinase 1 (CLK1) share close selectivity profiles [37], we next evaluated our hit against an extended panel of six additional cancer-related protein kinases including CLK1, cyclin-dependent kinase 5 (CDK5/p25), non-receptor tyrosine kinase ABL1, and the tyrosine kinases JAK3, ephrin type-B receptor 1 (EphB1) and epidermal growth factor receptor (EGFR). As expected, **MH-124** also inhibited CLK1 (IC_{50} value of 87 nM). However, no or only a slight inhibition was noticed for CDK5/p25, ABL1, JAK3, EphB1 and EGFR.

Table 2. Inhibitory activities (in black) and selected IC_{50} values (in green) of synthesized compounds against a panel of cancer-related protein kinases. The table displays the percentages of remaining kinase activities, detected after treatment with 10 μM of the tested compounds. The values obtained after treatment with 1 μM are given in brackets. Results are expressed in % of maximal activity, i.e. measured in the absence of inhibitor but with an equivalent dose of DMSO (solvent of the tested compounds). ATP concentration used in the kinase assays was 10 μM (values are means, n = 2). Kinases are from human origin except when it is specified *Rn*, *Rattus norvegicus*.

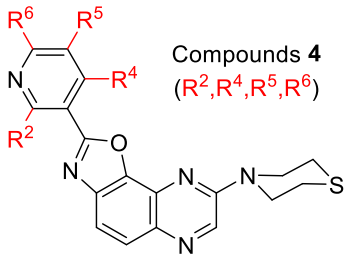 Compounds **4** (R^2,R^4,R^5,R^6)	CDK9/CyclinT	PIM1	DYRK1A	GSK-3α	GSK-3β	CK1ε	Haspin	VEGFR2	[a]
CD-07 (H,H,H,H) [17]	4 (69)	18 ([b])	5 (19)[c]	130[d]	0 (0)	4.8[d]	21 (14)	22[d]	44 (86)	8 (63)	-	4.6
4-2Me (Me,H,H,H)	32 (61)	22 (76)	13 (57)	6 (27)	-	11 (55)	-	32 (83)	33 (73)	63 (76)	-	
4-2OMe (OMe,H,H,H)	66 (79)	70 (77)	51 (60)	29 (46)	-	41 (75)	-	84 (90)	83 (84)	67 (69)	-	
4-2Cl (Cl,H,H,H)	32 (60)	48 (64)	18 (36)	14 (14)	173[d]	19 (22)	434[d]	86 (87)	50 (75)	99 (63)	2.5	
4-2F (F,H,H,H)	39 (34)	62 (44)	11 (9)[c]	3 (3)	32[d]	8 (9)	41[d]	[b] (99)	62 (51)	91 (93)	1.3	
4-2NMe$_2$ (NMe_2,H,H,H)	10 (36)	71 (77)	34 (83)	14 (42)	-	23 (70)	-	81 ([b])	80 (94)	67 (81)	-	
4-2pyrro ( ,H,H,H)	11 (54)	77 (79)	54 (72)	30 (58)	-	56 (81)	-	85 ([b])	81 (73)	[b] (76)	-	
4-4iPr (H,iPr,H,H)	1 (14)	[b] ([b])	0 (20)[c]	0 (2)	23[d]	0 (8)	32[d]	86 ([b])	37 (87)	95 ([b])	1.4	
4-4CF$_3$ (H,CF_3,H,H)	75 (47)	78 (69)	55 (21)	12 (10)	127[d]	18 (13)	123[d]	87 (93)	[b] (67)	59 (67)	1.0	
4-5Me (H,H,Me,H)	8 (40)	6 (35)	4 (20)	5 (5)	32[d]	4 (6)	85[d]	54 (90)	16 (37)	29 (66)	2.7	
4-5F (H,H,F,H)	51 (69)	68 (91)	11 (37)[c]	3 (8)	246[d]	15 (25)	359[d]	[b] ([b])	66 (89)	[b] (97)	1.5	
4-5Br (H,H,Br,H)	56 (75)	65 (82)	8 (38)[c]	0 (0)	115[d]	0 (9)	263[d]	89 (98)	41 (65)	86 ([b])	2.3	
4-5thienyl (H,H,  ,H)	24 (73)	21 ([b])	0 (48)[c]	0 (7)	51[d]	0 (31)	168[d]	69 ([b])	22 (91)	22 (56)	3.3	
4-5Smorpho (H,H,  ,H)	18 (49)	19 (71)	5 (32)[c]	2 (5)	119[d]	4 (11)	239[d]	87 ([b])	28 (64)	67 (71)	2.0	
4-6Cl (H,H,H,Cl)	55 (73)	[b] (84)	68 (54)[c]	0 (3)	530[d]	0 (33)	1100[d]	95 (96)	62 (91)	95 (96)	2.1	
4-6NMe$_2$ (H,H,H,NMe_2)	69 (83)	79 ([b])	52 (72)	3 (32)	-	16 (60)	-	85 ([b])	92 (89)	[b] (78)	-	
4-6Me (H,H,H,Me)	47 (61)	70 (82)	8 (26)[c]	0 (0)	89[d]	0 (0)	194[d]	92 (95)	48 (68)	96 (99)	2.2	
4-6ethinyl (H,H,H,C≡CH)	63 ([b])	[b] ([b])	90 ([b])[c]	10 (43)	-	24 (83)	-	94 ([b])	82 ([b])	98 ([b])	-	

[a] IC_{50}(GSK-3β)/IC_{50}(GSK-3α) as an evaluation of the isoform selectivity. [b] ≥100. [c] *Rn*DYRK1A. [d] IC_{50} (nM).

Table 2 (continued).

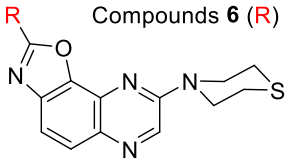 Compounds **6** (R)	CDK9/ CyclinT	PIM1	DYRK1A	GSK-3α	GSK-3β	CK1ε	Haspin	VEGFR2	[a]
FL-316 () [17]	9 (26)	12 (40)	4 (24)[c]	447[d]	2 (5)	31[d]	8 (9)	50[d]	78 ([b])	16 (48)	-	1.6
6-quino (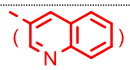)	87 (91)	97 (85)	54 (85)	-	13 (28)	-	19 (49)	-	95 (91)	[b] (84)	[b] (85)	-
6-isoquino (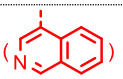)	28 (58)	64 (88)	5 (18)[c]	-	3 (9)	260[d]	4 (18)	670[d]	56 ([b])	26 (69)	58 (90)	2.6
6-pyra ()	23 (56)	6 (29)	6 (26)[c]	-	4 (5)	195[d]	14 (14)	310[d]	54 ([b])	14 (46)	52 (97)	1.6
6-thia ()	14 (56)	11 (58)	5 (54)	-	5 (16)	-	6 (17)	-	48 (91)	9 (49)	59 ([b])	-
6-isothia ()	28 (78)	33 (85)	16 (62)[c]	-	1 (23)	-	11 (41)	-	60 (96)	23 (69)	65 ([b])	-

Table 2 (continued).

Compounds **10** and **14** (X;R)	CDK9/ CyclinT	PIM1	DYRK1A	GSK-3α	GSK-3β	CK1ε	Haspin	VEGFR2 [a]	
FL-291 (N;N-O) [17]	27 (45)	23 (43)	3 (11)[c]	200[d]	9 (9)	15[d]	2 (2)	25[d]	65 (75)	-	-	1.7
CD-07 (N;N-S) [17]	4 (69)	18 ([b])	5 (19)[c]	130[d]	0 (0)	4.8[d]	21 (14)	22[d]	44 (86)	8 (63)	-	4.6
10-Smorpho (CH;N-S)	13 (27)	21 (43)	4 (12)[c]	-	5 (8)	70[d]	9 (13)	103[d]	71 (90)	10 (23)	65 (94)	1.5
10-H (CH;H)	55 (69)	26 (53)	0 (10)	132[d]	24 (79)	-	33 (75)	-	67 ([b])	4 (23)	41 (97)	-
14-H (N;H)	59 (71)	86 ([b])	8 (29)[c]	-	20 (66)	-	43 (82)	-	82 (96)	22 (48)	[b] ([b])	-
14-Cl (N;Cl)	91 (90)	67 (85)	25 (54)[c]	-	40 (73)	-	46 (80)	-	[b] ([b])	60 (94)	84 ([b])	-
14-thiazo (N; N-S)	20 (58)	23 (71)	2 (15)[c]	68[d]	3 (6)	17[d]	7 (10)	239[d]	60 (87)	7 (27)	25 (84)	14

Table 2 (continued).

	CDK5/p25	ABL1	CLK1	JAK3	EphB1	EGFR
14-thiazo or MH-124	63 (92)	78 (96)	11 (27)	87[d]	79 (72)	81 (96)	98 ([b])

In general, docking studies revealed that most compounds exhibited a good fit in the binding sites of GSK-3α and -3β. The unsubstituted compound **4** (**CD-07**) showed a strong hydrogen bond with Lys148(85) of GSK-3α(β), an interaction that appears to be essential for ligand binding. Substitutions at the pyridine 2-position caused a slight change in ring orientation, leading to the loss of the hydrogen bond with the Lys amino acid. Only a small substituent such as 2-chloro kept the ring in place and thus maintained this hydrogen bond. However, the bioactivity of **4-2Cl** and **4-2F** were found lower than that of **CD-07**, possibly due to the electron-withdrawing properties of halogens which may weaken this interaction. Substitutions at the pyridine 4- and 5-positions are allowed because these regions face an open solvent-exposed area of the binding sites, with those at the 4-position allowing more variation than those at the 5-position. Substitutions at the 5- and particularly the 6-position of pyridine are closer to the amino acids, and large substituents may lead to clashes with surrounding amino acids or rotation of the

pyridine ring to lose the essential hydrogen bond. Generally, the compounds **4** showed binding to the GSK-3α isoform with slightly more favorable energetics.

Substitutions with rings other than pyridine, as in case of the compounds **6**, resulted in losing the hydrogen bond with the Lys residue (this is retained in the case of **FL-316** possessing an imidazole); this reflects the observed results of GSK-3 inhibition.

The region occupied by the fused ring is mostly hydrophobic with one nitrogen pointing perfectly to a highly polar spot in the binding site, while the other nitrogen (CH in **10-H**) is in a general hydrophobic region with polar spots within ~4.5 Å. This last nitrogen seems to be necessary to increase the interactions displayed by the first nitrogen and to facilitate the displacement of water because its replacement by a CH (compound **10-H**) was accompanied by a loss of the activity on kinase. Substitutions (R groups) are tolerated because the binding pocket has a wide and open region at this end to accommodate different types of large, and especially polar, substituents. Differences in size and polarity at the region occupied by the thiazolidine in the binding pocket may be responsible for the high selectivity of **MH-124** toward GSK-3α compared to GSK-3β. Thiazolidine fits more naturally into the thermodynamic map of GSK-3α, which has a marginally higher polarity in this region than GSK-3β (Figure 5). On the other hand, **CD-07** possesses a thiomorpholine which is slightly larger than thiazolidine and therefore does not possess sufficient polarity to match the chemical environment of the specific region of GSK-3α.

2.5. Activity of MH-124 (14-thiazo) on glioblastoma cells

We finally evaluated the efficacy of **MH-124** alone and in combination with temozolomide (TMZ) in two glioblastoma (GBM) patient-derived cell lines (PDCLs) that were selected to represent diverse response to TMZ i.e. N15-0385 (IC_{50} > 1000 μM) and 4339 (IC_{50} = 429.7 μM). Both PDCLs express GSK-3α and GSK-3β at a similar level than the whole collection of GlioTEx's 26 fully characterized GBM PDCLs (see Supplementary data). **MH-124** alone did not dramatically impact cell survival in both PDCLs, as the IC_{50} values were not reached at the highest concentration tested (0.5 μM; Figure 9), although the viability of 4339 PDCL was reduced of 45% when exposed to this concentration.

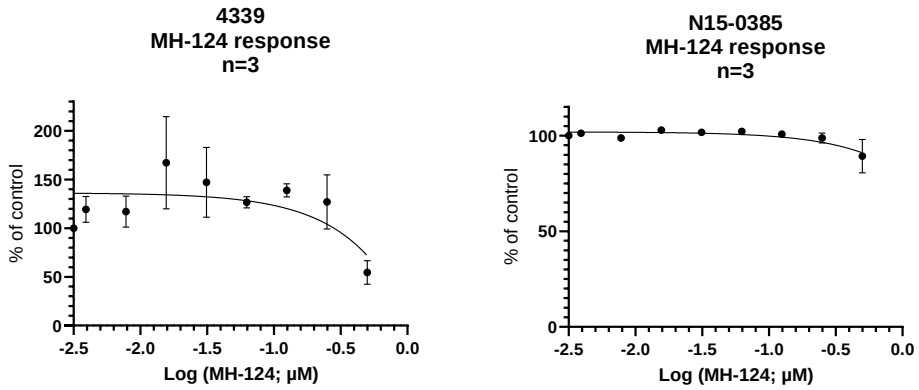

Figure 9. Impact of **MH-124** on 4339 (left) and N15-0385 (right) GBM cells. *In vitro* cell proliferation of GBM patient-derived cell line (PDCL) 4339 and N15-0385 as measured using Wst-1 assay. Y-axis represents optical density following 120 h of exposure to **MH-124** compared to untreated condition. Data are means of three independent experiments.

The impact of **MH-124** on TMZ efficacy was then evaluated. Dose-response curves were generated using 8 concentrations of TMZ ranging from 25 to 1000 µM, and 5 concentrations of **MH-124** ranging from 0.03 to 0.5 µM (Figure 10). Viability values for each condition are also represented in heatmaps (Figure 11).

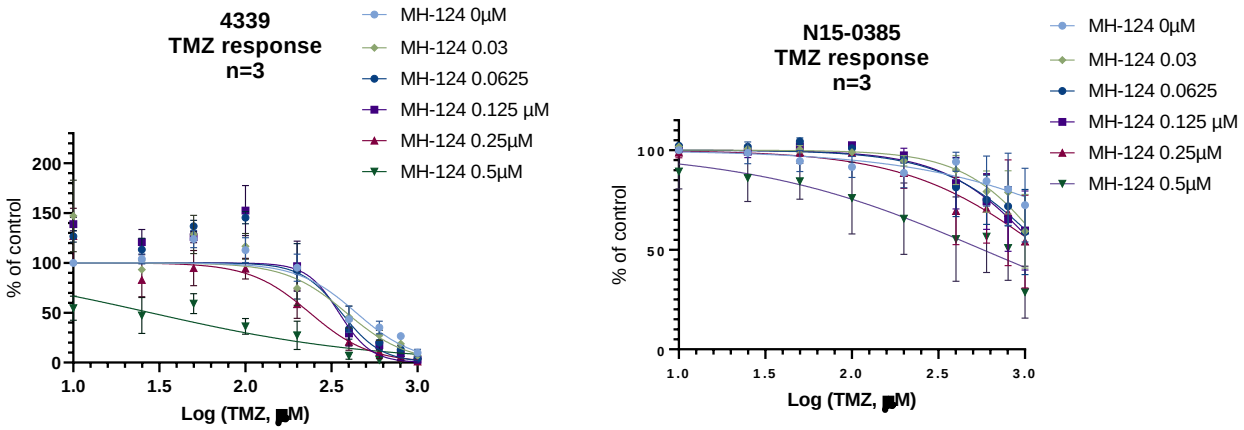

Figure 10. Impact of **MH-124** on TMZ efficacy. *In vitro* cell proliferation of GBM PDCL 4339 and N15-0385 as measured using Wst-1 assay. Y-axis represents optical density following 120 h of exposure to TMZ combined or not with **MH-124** compared to untreated condition. Data are means of three independent experiments.

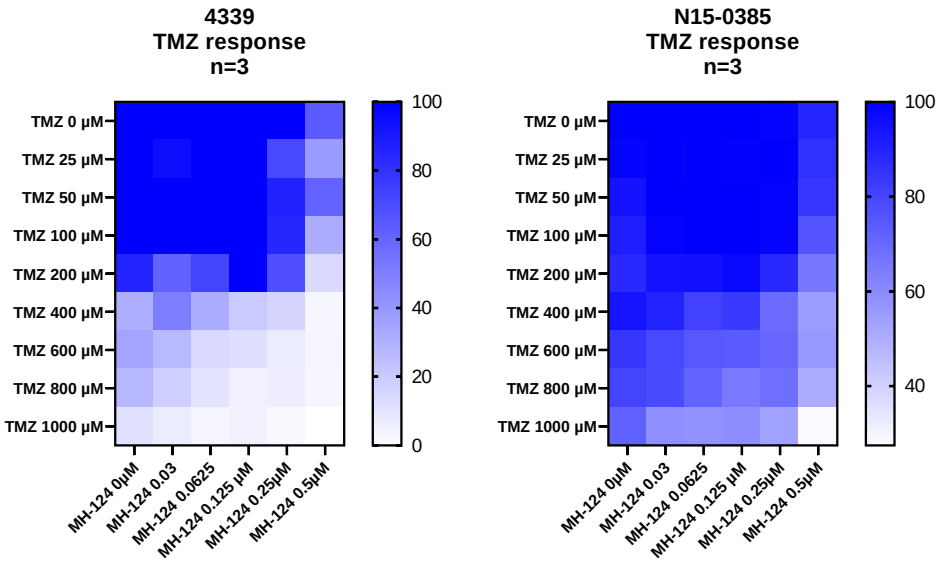

Figure 11. Heatmap representation of data shown in Figure 10 showing the impact of **MH-124** on TMZ efficacy in GBM PDCL 4339 (left) and N15-0385 (right).

The IC_{50} values obtained from these data show that the addition of **MH-124** to TMZ effectively reduced the IC_{50} values for both PDCLs (Figure 12). Indeed, in 4339, TMZ IC_{50} was reduced of 10-fold when **MH-124** was added at 0.5 µM. In N15-0385, it was reduced of more than 2-fold at the same concentration, transforming this TMZ-resistant PDCL (i.e. IC_{50} not reached) into a responder PDCL (IC_{50} = 573.5 µM).

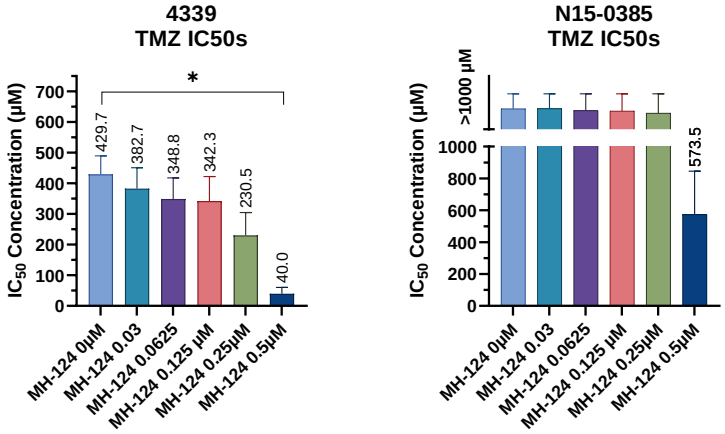

Figure 12. IC_{50} derived from data shown in Figure 10 showing the impact of **MH-124** on TMZ efficacy in GBM PDCL 4339 (left) and N15-0385 (right).

Synergy analyses using Bliss model (Figure 13) suggest that both drugs act synergistically at all concentrations for 4339 (i.e. synergy score ≥ 10). For N15-0385, synergy was observed at TMZ

concentrations above 400 µM and **MH-124** concentrations above 0.06 µM. Concentrations below these values were calculated as additive (i.e. synergy score between -10 and 10) in this PDCL according to the Bliss model.

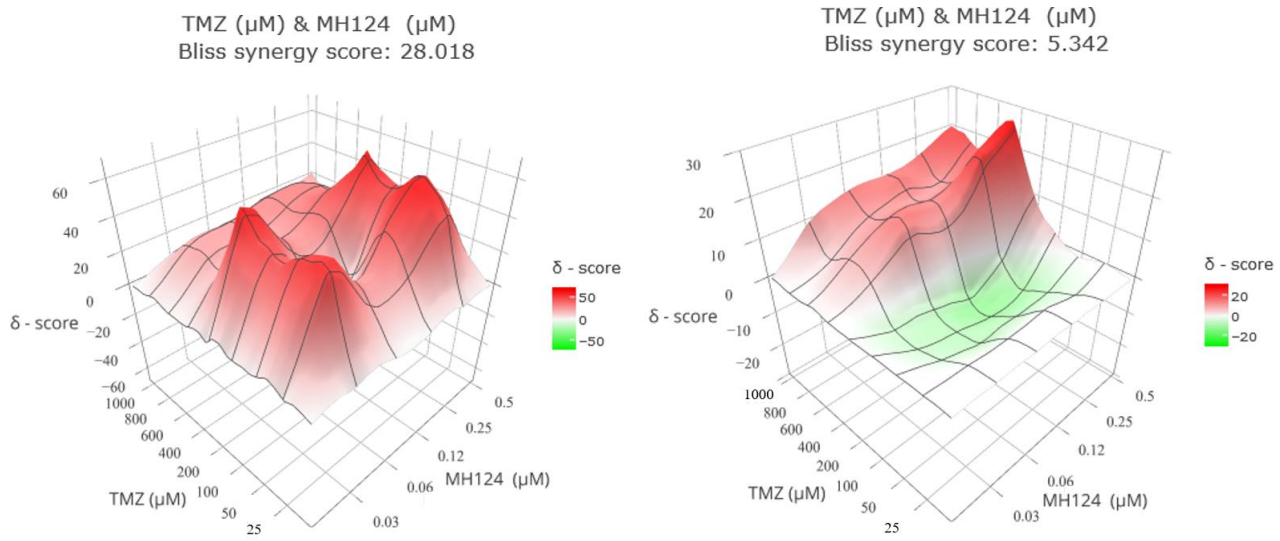

Figure 13. Synergy analyses of data shown in Figure 10 using Bliss model for GBM PDCL 4339 (left) and N15-0385 (right) cells.

3. Conclusion and perspectives

Since the biological function and regulation of the two isoforms of GSK-3 are distinct (the α isoform does not enter the nucleus and does not contribute to the elevation of β-catenin), the development of selective inhibitors is of main importance. While few specific GSK-3α inhibitors are in development, we were here able to identify a powerful one, **MH-124**, owing to co-crystallization in GSK-3β and docking studies in accurate models of GSK-3α. **MH-124** not only benefits from a simple synthesis route, but is 14 times more potent at inhibiting GSK-3α than the β isoform.

In the frame of this work, we were also able to demonstrate the interest of combining **MH-124** as a new inhibitor of GSK-3α with temozolomide (TMZ) to treat a resistant cell line of GBM which is an aggressive malignancy. While the ability of GSK-3 inhibitors to promote apoptosis and cell cycle arrest in brain cancer cell was already known, only contrasting results had been reported as to the nature of the responsible isoform. Our study showed the interest of inhibiting the isoform α of GSK-3 to restore the efficacy of TMZ treatment on resistant GBM cells.

However, further work remains to be done to better understand the mechanism of action of our lead compound. Notably, as the human protein kinase superfamily consists of 518 members, one of our future goals will be to perform a more comprehensive kinase screen with **MH-124** [38]. Its toxicity on non-cancer cells will also remain to be evaluated. Finally, many more applications could be expected for this compound, in the field of cancer and far beyond since the GSK-3 kinase is implicated in many diseases related to cardiac pathogenesis, atherosclerosis, metabolic disorders, tissue aging, regulation of solid and hematological malignancies, and neurodegenerative disorders.

4. Experimental

4.1. Toxicity study

4.1.1. Culture of neuronal cells

NSC-34 cells were obtained from the ATCC (Manassas, VA). Cells were grown in DMEM (Invitrogen, San Diego, CA), pH 7.4, supplemented with 10% heat-inactivated FCS (Biochrom KG, Berlin, Germany), 100 units.mL^{-1} penicillin and 100 µg.mL^{-1} streptomycin. Cells were plated (40,000 cells/cm^2) and cultured at 37 °C in a humidified atmosphere with 5% CO_2. Cells were harvested by incubation for 5 min with 0.05% (w/v) trypsin (Sigma Aldrich, St. Louis, MO) in PBS, pH 7.4, containing 0.3 mM EDTA, followed by the addition of 10% FCS to inactivate the trypsin. Cells were allowed to attach for 24 h before any treatment addition.

Primary cultures of cortical neurons were prepared from the cerebral cortex of 14-15-day old rat fetuses (5 female rats to obtain the fetuses). The cerebral cortex, obtained under toxin-free sterile conditions, was dissected and dissociated mechanically by pipetting 10 times with DMEM (10 mL for the cortex obtained from 12-14 fetuses). The cell suspension was filtered through a nylon mesh with a pore size of 90 µm and plated (5 x 10^4 cells/cm^2) on poly-lysine-coated dishes. After the cell attachment (1 h), the plating medium was changed to DMEM pH 7.4, supplemented with 10% fetal bovine serum (FBS), 10 mM HEPES, 40 mM $NaHCO_3$, 100 units.mL^{-1} penicillin, and 100 mg.mL^{-1} streptomycin. One hour is

enough to stick neurons and to avoid astrocytes sticking on the plate. After 4 days, the plating medium was changed with another medium prepared as described above. At seven days of culture, 20% FBS was changed to a 10% solution. Cultures were grown in a humidified atmosphere of 5% CO_2 and 95% O_2, at 37 °C for 3 days, and then exposed to cytosine β-D arabinofuranoside (10 μM) for 24 h to prevent proliferation of no neuronal cells. Possible contamination by astrocytes was assessed by immuno-fluorescence using monoclonal anti-glial fibrillary acidic protein (GFAP) (astrocytes marker: Sigma-Aldrich 1:500) antibody (clone G-A-5) and polyclonal anti-microtubule associated protein 2 (MAP-2) (neuronal marker: Sigma-Aldrich 1:500). Under these conditions, approximately 99% ± 3% of all cultured cells were neurons. All animal work was performed according to minimize animal suffering and to reduce the total number of animals used.

4.1.2. MTT assay

Cell viability of the cultures was determined by the MTT assay as previously reported [39]. Cells were plated in 96 well culture plate and incubated without or with **FL-291** during 24 h at 10 μM, 20 μM, 40 μM, 80 μM or 160 μM. After cell treatments, the medium was removed, and the cells were incubated with red free medium and MTT solution [0.5 $mg.mL^{-1}$ prepared in phosphate buffer saline (PBS) solution] for 4 h at 37 ºC. Finally, the medium was removed, and formazan particles were dissolved in DMSO. NSC-34 cell viability, defined as the relative amount of MTT reduction, was determined by spectrophotometry at 570 nm.

4.1.3. Trypan blue assay

Trypan blue exclusion assay was used to count living cells and death cells. NSC-34 cells were isolated and seeded at $4x10^4$ cells/35 mm dish. After 5 days of culture, cells were incubated without (control, C) or with 20 μM, 40 μM, 80 μM or 160 μM **FL-291** for 24 h. 1.5% trypan blue solution was applied to NSC-34 cultures at rt for 3 min. Living and dead cells were counted accurately with a Countess Automated Cell Counter (Invitrogen, Carlsbad, CA, USA).

4.1.4. Confocal microscopy

NSC-34 monolayers growing on 16-mm glass coverslips for 6 h were prepared for confocal studies. Cultures were grown in a humidified atmosphere of 5% CO_2/95% air at 37 °C before prepared cells to confocal.

4.1.5. Statistical analysis

Data was expressed as the mean ± SD values. Statistical significance was determined using the Mann-Withney test or one-way Anova. For multiple comparisons, Tukey's tests were used as post hoc tests or Kruskal-Wallis test for appropriate analyses. For all analyses, p values < 0.05 were considered significant. The type of statistical test is specified in each figure legend.

4.2. Protein crystallography

Recombinant kinase domain of GSK-3β containing a C-terminal His-tag was expressed in *E. coli*. The protein was purified by Ni^{2+} affinity chromatography and subsequently size exclusion chromatography. The pure protein in 20 mM HEPES, pH 7.5, 200 mM NaCl and 2 mM DTT was concentrated to 10 $mg.mL^{-1}$, and was mixed with the inhibitor at 1 mM. Crystallization was carried out using sitting drop vapor diffusion method at 4 °C and the conditions containing 14% PEG 3350, 0.1 M ammonium sulfate and 0.1 M bis-tris pH 6.0 with and without a supplementation of 5% glycerol. The crystals were cryo-protected with the mother liquor supplemented with 22% ethylene glycol. Diffraction data were collected at Swiss Light Source beamline X06DA. The data were processed with iMosflm [40], and scaled using aimless [41]. Molecular replacement was performed using Phaser [42] and the published GSK-3β structure (pdb id 1q3d [43]). The structures were subjected to manual model rebuilding and refinement using COOT [44] and REFMAC5 [45], respectively. The data collection and refinement statistics are summarized in Table S3. The pdb IDs are 8AV1 for **CD-07** and 8AUZ for **FL-291**.

4.3. Molecular modeling experiments

The crystal structure of GSK-3β was obtained from the protein databank (PDB ID: 4ACC) [46]. The 3D structure of GSK-3α was constructed using the default options in Prime [23, 47]. The homology

model was compared to the one deposited in the AlphaFold database [23, 47]. The ligands were sketched and minimized in Maestro [48], and LigPrep [49] was used to prepare the ligands for the docking step. The protein structures were prepared by the Protein Preparation Wizard [50, 51] to adjust the bond orders, add missing atoms, complete missing side chains and loops, and adjust the hydrogen bond network. Docking experiments were carried out by Glide SP [52-55]. Water thermodynamics were computed using SZMAP [56].

4.4. General data regarding the synthesis of the targets

Column chromatography separations were achieved on silica gel (40-63 μm). Melting points were measured on a Kofler apparatus. IR spectra were taken on a Perkin-Elmer Spectrum 100 spectrometer. ^{1}H and ^{13}C Nuclear Magnetic Resonance (NMR) spectra were recorded either on a Bruker Avance III spectrometer at 300 MHz and 75 MHz respectively, on a Bruker Avance III spectrometer at 400 MHz and 100 MHz respectively, or on a Bruker Avance III HD spectrometer at 500 MHz and 126 MHz respectively, all fitted with a BBFO probe. ^{1}H chemical shifts (δ) are given relative to the solvent residual peak and ^{13}C chemical shifts are relative to the central peak of the solvent signal [57].

3-Chloro-5-iodo-6-quinoxalinamine (**1**) [17], ethyl 4-isopropylnicotinate [58] and 5-iodo-6-quinoxalinamine (**12**) [25] were prepared as described previously.

When not available from commercial sources, the substituted nicotinic acids were prepared from the corresponding ethyl nicotinates (1.5 mmol) by reaction with an aqueous 2 M solution of sodium hydroxide (0.83 mL, 1.65 mmol) in dioxane (2 mL) at 60 °C for 1 h. After evaporation of the solvent under reduced pressure, the residue was diluted with water (7 mL) and acidified with an aqueous 1 M solution of hydrochloric acid until pH 6. The precipitate was collected by filtration, dried under vacuum, and used directly.

When not available from commercial sources, the aroyl chlorides were prepared from the corresponding carboxylic acids (1.5 mmol) by reaction with oxalyl chloride (0.21 g, 0.14 mL, 1.65 mmol) in dichloromethane (2 mL) containing dimethylformamide (10 μL) at rt for 2 h. They were used directly

after removal of the solvent under reduced vacuum, addition of toluene (10 mL), and removal of the solvent under reduced vacuum.

4.5. Evaluation on kinases

The enzymatic activities of CDK5/p25, CDK9/Cyclin T, PIM1, DYRK1A, GSK-3 isoforms α and/or β, CK1 isoforms ε, Haspin, ABL1, JAK3, CLK1 and VEGFR were assayed using the ADP-Glo™ assay kit (Promega, Madison, WI) as previously described [36]. Human EGFR and EphB1 (both are recombinant, expressed by baculovirus in Sf9 insect cells) were assayed in kinase buffer "A" with 0.17 $\mu g.\mu L^{-1}$ of poly(L-glutamic acid – L-tyrosine) sodium salt as substrate. Kinase buffer "A": 10 mM $MgCl_2$, 1 mM EGTA, 1 mM DTT, 25 mM Tris-HCl pH 7.5, 50 $\mu g.mL^{-1}$ heparin. This ADP-Glo™ assay is a luminescent ADP detection assay that provides a homogeneous and high-throughput screening method to measure kinase activity by quantifying the amount of ADP produced during the enzymatic reaction. ATP concentration used in the kinase assays was 10 µM.

4.6. Evaluation on glioblastoma cell lines

4.6.1. Cell lines. All GBM PDCLs were established by the GlioTEx team (Glioblastoma and Experimental Therapeutics) in the Paris Brain Institute (ICM) laboratory and maintained at 37 °C, 5% CO_2 under neurosphere growth conditions using DMEM/F12 (Gibco, Life Technologies, Saint-Aubin, France) culture medium supplemented with 1% penicillin/streptomycin, B27 diluted 1:50 (Gibco), EGF (20 $ng.mL^{-1}$), and FGF (20 $ng.mL^{-1}$) (Preprotech, Neuilly-sur-Seine, France). The identity of all cell lines established at the ICM was confirmed by short tandem repeat (STR) assay according to the manufacturer's instructions (PowerPlex 16, Promega, Charbonnières-les-Bains, France). PCR products were sent to Genoscreen (Lille, France) to determine STR profiles. The profiles were compared to the parental tumors and validated within three months of their use for the studies presented here.

4.6.2. Cell viability assay. All tests described were performed in three independent experiments: 384-well plates were coated with 10 $\mu g.mL^{-1}$ laminin (#L2020, Sigma–Aldrich, Saint-Quentin Fallavier,

France) at 37 °C for 1 h. Two thousand five hundred cells/well were then plated in full culture medium. **MH-124** or temozolomide were added the next day from 30 µM and 51.5 mM stock solutions, respectively, in DMSO, using epMotion ® 5070 automated pipetting robot (Eppendorf, Montesson, France). Ninety-six hours later, cell viability was assessed using WST-1 reagent (Roche, Meylan, France) according to the manufacturer's instructions.

4.6.3. Synergy analysis. The expected drug combination responses were calculated based on Bliss reference model using SynergyFinder [59]. Deviations between observed and expected responses with positive and negative values denote synergy and antagonism respectively. The Bliss independence model assumes a stochastic process in which two drugs elicit their effects independently, and the expected combination effect can be calculated based on the probability of independent events. A score less than -10: the interaction between two drugs is likely to be antagonistic; From -10 to 10: the interaction between two drugs is likely to be additive; Larger than 10: the interaction between two drugs is likely to be synergistic.

Acknowledgments. F. L., W. E. and F. M. thank the "Comité d'Ille et Vilaine 35" de la Ligue Contre le Cancer, the Université de Rennes 1 and the Centre National de la Recherche Scientifique for supporting this research. A. S. gratefully acknowledges the Tunisian Ministry of Higher Education and Scientific Research for the financial support (grant for M. H.). S. B. and T. R. thank the Cancéropôle Grand Ouest ("Marine molecules, metabolism and cancer" network), IBiSA (French Infrastructures en sciences du vivant: biologie, santé et agronomie) and Biogenouest (Western France life science and environment core facility network supported by the Conseil Régional de Bretagne) for supporting the KISSf screening facility (FR2424, CNRS and Sorbonne Université). M. N. and K. M. E. thank OpenEye Scientific Software for granting the permission to use SMAP. The research conducted at Temple University includes calculations carried out on HPC resources supported in part by the National Science Foundation

through major research instrumentation grant number 1625061 and by the US Army Research Laboratory under contract number W911NF-16-2-0189.

Supplementary data. Supplementary data associated with this article can be found online at http://doi.org/10.1016/j.bioorgxxxxxxxxxxx.

References and Notes

[1] S. Klaeger, S. Heinzlmeir, M. Wilhelm, H. Polzer, B. Vick, P.-A. Koenig, M. Reinecke, B. Ruprecht, S. Petzoldt, C. Meng, J. Zecha, K. Reiter, H. Qiao, D. Helm, H. Koch, M. Schoof, G. Canevari, E. Casale, S.R. Depaolini, A. Feuchtinger, Z. Wu, T. Schmidt, L. Rueckert, W. Becker, J. Huenges, A.-K. Garz, B.-O. Gohlke, D.P. Zolg, G. Kayser, T. Vooder, R. Preissner, H. Hahne, N. Tonisson, K. Kramer, K. Goetze, F. Bassermann, J. Schlegl, H.-C. Ehrlich, S. Aiche, A. Walch, P.A. Greif, S. Schneider, E.R. Felder, J. Ruland, G. Medard, I. Jeremias, K. Spiekermann, B. Kuster, The target landscape of clinical kinase drugs, Science 358(6367) (2017) 1148, doi: 10.1126/science.aan4368.

[2] R. Roskoski, Jr., Properties of FDA-approved small molecule protein kinase inhibitors: A 2021 update, Pharmacol. Res. 165 (2021) 105463, doi: 10.1016/j.phrs.2021.105463.

[3] M.M. Attwood, D. Fabbro, A.V. Sokolov, S. Knapp, H.B. Schioeth, Trends in kinase drug discovery: targets, indications and inhibitor design, Nat. Rev. Drug Discov. 20(11) (2021) 839-861, 10.1038/s41573-021-00252-y.

[4] M.K. Pandey, T.R. DeGrado, Glycogen synthase kinase-3 (GSK-3)-targeted therapy and imaging, Theranostics 6(4) (2016) 571-593, doi: 10.7150/thno.14334.

[5] A. Prasanth Saraswati, S.M. Ali Hussaini, N. Hari Krishna, B. Nagendra Babu, A. Kamal, Glycogen synthase kinase-3 and its inhibitors: Potential target for various therapeutic conditions, Eur. J. Med. Chem. 144 (2018) 843-858, doi: 10.1016/j.ejmech.2017.11.103.

[6] L. Wang, J. Li, L.-j. Di, Glycogen synthesis and beyond, a comprehensive review of GSK3 as a key regulator of metabolic pathways and a therapeutic target for treating metabolic diseases, Med. Res. Rev. (2021) 1-37, doi: 10.1002/med.21867.

[7] Y. Zhang, X. Wang, Targeting the Wnt/β-catenin signaling pathway in cancer. FIELD Authors:Zhang, Ya; Wang, Xin, J. Hematol. Oncol. 13(1) (2020) 165, 10.1186/s13045-020-00990-3.

[8] V.S. Tomar, V. Patil, K. Somasundaram, Temozolomide induces activation of Wnt/β-catenin signaling in glioma cells via PI3K/Akt pathway: implications in glioma therapy, Cell Biology and Toxicology 36(3) (2020) 273-278, 10.1007/s10565-019-09502-7.

[9] O. Silva-García, R. Cortés-Vieyra, F.N. Mendoza-Ambrosio, G. Ramírez-Galicia, V.M. Baizabal-Aguirre, GSK3α: an important paralog in neurodegenerative disorders and cancer, Biomolecules 10(12) (2020) 1683, doi: 10.3390/biom10121683.

[10] F. Ahmad, J.R. Woodgett, Emerging roles of GSK-3α in pathophysiology: Emphasis on cardio-metabolic disorders, Biochim. Biophys. Acta, Mol. Cell Res. 1867(2) (2020) 118616, doi: 10.1016/j.bbamcr.2019.118616.

[11] S. Shang, F. Hua, Z.-W. Hu, The regulation of β-catenin activity and function in cancer: therapeutic opportunities, Oncotarget 8(20) (2017) 33972-33989, doi: 10.18632/oncotarget.15687.

[12] F.F. Wagner, L. Benajiba, A.J. Campbell, M. Weiewer, J.R. Sacher, J.P. Gale, L. Ross, A. Puissant, G. Alexe, A. Conway, M. Back, Y. Pikman, I. Galinsky, D.J. Deangelo, R.M. Stone, T. Kaya, X. Shi, M.B. Robers, T. Machleidt, J. Wilkinson, O. Hermine, A. Kung, A.J. Stein, D.

Lakshminarasimhan, M.T. Hemann, E. Scolnick, Y.-L. Zhang, J.Q. Pan, K. Stegmaier, E.B. Holson, Exploiting an Asp-Glu "switch" in glycogen synthase kinase 3 to design paralog-selective inhibitors for use in acute myeloid leukemia, Sci. Transl. Med. 10(431) (2018) eaam8460, doi: 10.1126/scitranslmed.aam8460.

[13] P.K. McCamphill, L.J. Stoppel, R.K. Senter, M.C. Lewis, A.J. Heynen, D.C. Stoppel, V. Sridhar, K.A. Collins, X. Shi, J.Q. Pan, J. Madison, J.R. Cottrell, K.M. Huber, E.M. Scolnick, E.B. Holson, F.F. Wagner, M.F. Bear, Selective inhibition of glycogen synthase kinase 3α corrects pathophysiology in a mouse model of fragile X syndrome, Sci. Transl. Med. 12(544) (2020) eaam8572, doi: 10.1126/scitranslmed.aam8572.

[14] F. Lo Monte, T. Kramer, J. Gu, M. Brodrecht, J. Pilakowski, A. Fuertes, J.M. Dominguez, B. Plotkin, H. Eldar-Finkelman, B. Schmidt, Structure-based optimization of oxadiazole-based GSK-3 inhibitors, Eur. J. Med. Chem. 61 (2013) 26-40, doi: 10.1016/j.ejmech.2012.06.006.

[15] T. Neumann, L. Benajiba, S. Goering, K. Stegmaier, B. Schmidt, Evaluation of Improved Glycogen Synthase Kinase-3α Inhibitors in Models of Acute Myeloid Leukemia, J. Med. Chem. 58(22) (2015) 8907-8919, doi: 10.1021/acs.jmedchem.5b01200.

[16] Y. Wang, X. Dou, L. Jiang, H. Jin, L. Zhang, L. Zhang, Z. Liu, Discovery of novel glycogen synthase kinase-3α inhibitors: Structure-based virtual screening, preliminary SAR and biological evaluation for treatment of acute myeloid leukemia, Eur. J. Med. Chem. 171 (2019) 221-234, doi: 10.1016/j.ejmech.2019.03.039.

[17] F. Lassagne, C. Duguépéroux, C. Roca, C. Perez, A. Martinez, B. Baratte, T. Robert, S. Ruchaud, S. Bach, W. Erb, T. Roisnel, F. Mongin, From simple quinoxalines to potent oxazolo[5,4-f]quinoxaline inhibitors of glycogen-synthase kinase 3 (GSK3), Org. Biomol. Chem. 18(1) (2020) 154-162, doi: 10.1039/c9ob02002k.

[18] Y. Oda, Choline acetyltransferase: the structure, distribution and pathologic changes in the central nervous system, Pathol. Int. 49(11) (1999) 921-937, 10.1046/j.1440-1827.1999.00977.x.

[19] J.D. Rothstein, Current hypotheses for the underlying biology of amyotrophic lateral sclerosis, Ann. Neurol. 65(1) (2009) S3-S9, 10.1002/ana.21543.

[20] W. Zhang, M. Bai, Y. Xi, J. Hao, L. Liu, N. Mao, C. Su, J. Miao, Z. Li, Early memory deficits precede plaque deposition in APPswe/PS1dE9 mice: Involvement of oxidative stress and cholinergic dysfunction, Free Radical Biol. Med. 52(8) (2012) 1443-1452, 10.1016/j.freeradbiomed.2012.01.023.

[21] N.R. Cashman, H.D. Durham, J.K. Blusztajn, K. Oda, T. Tabira, I.T. Shaw, S. Dahrouge, J.P. Antel, Neuroblastoma x spinal cord (NSC) hybrid cell lines resemble developing motor neurons. FIELD Authors:, Dev. Dyn. 194(3) (1992) 209-21, 10.1002/aja.1001940306.

[22] S. Prasanna, P.R. Daga, A. Xie, R.J. Doerksen, Glycogen synthase kinase-3 inhibition by 3-anilino-4-phenylmaleimides: insights from 3D-QSAR and docking, J. Comput. Aided Mol. Des. 23(2) (2009) 113-127, doi: 10.1007/s10822-008-9244-1.

[23] J. Jumper, R. Evans, A. Pritzel, T. Green, M. Figurnov, O. Ronneberger, K. Tunyasuvunakool, R. Bates, A. Zidek, A. Potapenko, A. Bridgland, C. Meyer, S.A.A. Kohl, A.J. Ballard, A. Cowie, B. Romera-Paredes, S. Nikolov, R. Jain, J. Adler, T. Back, S. Petersen, D. Reiman, E. Clancy, M. Zielinski, M. Steinegger, M. Pacholska, T. Berghammer, S. Bodenstein, D. Silver, O. Vinyals, A.W. Senior, K. Kavukcuoglu, P. Kohli, D. Hassabis, Highly accurate protein structure prediction with AlphaFold, Nature 596(7873) (2021) 583-589, doi: 10.1038/s41586-021-03819-2.

[24] K. Tunyasuvunakool, J. Adler, Z. Wu, T. Green, M. Zielinski, A. Zidek, A. Bridgland, A. Cowie, C. Meyer, A. Laydon, S. Velankar, G.J. Kleywegt, A. Bateman, R. Evans, A. Pritzel, M. Figurnov, O. Ronneberger, R. Bates, S.A.A. Kohl, A. Potapenko, A.J. Ballard, B. Romera-Paredes, S. Nikolov, R. Jain, E. Clancy, D. Reiman, S. Petersen, A.W. Senior, K. Kavukcuoglu, E. Birney, P. Kohli, J. Jumper, D. Hassabis, Highly accurate protein structure prediction for the human proteome, Nature 596(7873) (2021) 590-596, doi: 10.1038/s41586-021-03828-1.

[25] F. Lassagne, J.M. Sims, W. Erb, O. Mongin, N. Richy, N. El Osmani, Z. Fajloun, L. Picot, V. Thiery, T. Robert, S. Bach, V. Dorcet, T. Roisnel, F. Mongin, Thiazolo[5,4-f]quinoxalines, Oxazolo[5,4-f]quinoxalines and Pyrazino[b,e]isatins: Synthesis from 6-Aminoquinoxalines and Properties, Eur. J. Org. Chem. (19) (2021) 2756-2763, 10.1002/ejoc.202100362.
[26] M.T. Morales-Colón, Y.Y. See, S.J. Lee, P.J.H. Scott, D.C. Bland, M.S. Sanford, Tetramethylammonium Fluoride Alcohol Adducts for SNAr Fluorination, Org. Lett. 23(11) (2021) 4493-4498, 10.1021/acs.orglett.1c01490.
[27] N. Miyaura, A. Suzuki, Palladium-Catalyzed Cross-Coupling Reactions of Organoboron Compounds, Chem. Rev. 95(7) (1995) 2457-2483, doi: 10.1021/cr00039a007.
[28] D. Schade, M. Lanier, E. Willems, K. Okolotowicz, P. Bushway, C. Wahlquist, C. Gilley, M. Mercola, J.R. Cashman, Synthesis and SAR of b-Annulated 1,4-Dihydropyridines Define Cardiomyogenic Compounds as Novel Inhibitors of TGFβ Signaling, J. Med. Chem. 55(22) (2012) 9946-9957, doi: 10.1021/jm301144g.
[29] J. Liu, J.B. Eaton, B. Caldarone, R.J. Lukas, A.P. Kozikowski, Chemistry and Pharmacological Characterization of Novel Nitrogen Analogues of AMOP-H-OH (Sazetidine-A, 6-[5-(Azetidin-2-ylmethoxy)pyridin-3-yl]hex-5-yn-1-ol) as α4β2-Nicotinic Acetylcholine Receptor-Selective Partial Agonists, J. Med. Chem. 53(19) (2010) 6973-6985, doi: 10.1021/jm100765u.
[30] J.L. Díaz, F. Cuevas, G. Pazos, P. Álvarez-Bercedo, A.I. Oliva, M.Á. Sarmentero, D. Font, A. Jiménez-Aquino, M. Morón, A. Port, R. Pascual, A. Dordal, E. Portillo-Salido, R.F. Reinoso, J.M. Vela, C. Almansa, Bicyclic Diazepinones as Dual Ligands of the α2δ-1 Subunit of Voltage-Gated Calcium Channels and the Norepinephrine Transporter, J. Med. Chem. 64(4) (2021) 2167-2185, doi: 10.1021/acs.jmedchem.0c01867.
[31] K. Sonogashira, Y. Tohda, N. Hagihara, Convenient synthesis of acetylenes. Catalytic substitutions of acetylenic hydrogen with bromo alkenes, iodo arenes, and bromopyridines, Tetrahedron Lett. (50) (1975) 4467-4470, doi: 10.1016/s0040-4039(00)91094-3.
[32] K.A. Yeboah, J.D. Boyd, K.A. Kyerematen, C.C. Shepherd, I.M. Ingersoll, D.L. Jackson, Jr., A.W. Holland, Large accelerations from small thermal differences: case studies and conventional reproduction of microwave effects on palladium couplings, React. Kinet., Mech. Catal. 112(2) (2014) 295-304, doi: 10.1007/s11144-014-0733-z.
[33] H.R. Khavasi, A.A. Tehrani, Effect of halogen bonding interaction on supramolecular assembly of halogen-substituted phenylpyrazinamides, CrystEngComm 15(16) (2013) 3222-3235, 10.1039/c3ce40093j.
[34] F. Zymalkowski, P. Tinapp, Chemistry of 3-quinolinecarboxaldehyde, Justus Liebigs Ann. Chem. 699 (1966) 98-106, doi: 10.1002/jlac.19666990110.
[35] F. Trécourt, F. Mongin, M. Mallet, G. Queguiner, Substituted 8-methoxyquinolines - Regioselective bromination, coupling reactions and cyclization to an 11H-indolo[3,2-c]quinoline, Synth. Commun. 25(24) (1995) 4011-4024,
[36] N. Mokhtari Brikci-Nigassa, G. Bentabed-Ababsa, W. Erb, F. Chevallier, L. Picot, L. Vitek, A. Fleury, V. Thiéry, M. Souab, T. Robert, S. Ruchaud, S. Bach, T. Roisnel, F. Mongin, 2-Aminophenones, a common precursor to N-aryl isatins and acridines endowed with bioactivities, Tetrahedron 74(15) (2018) 1785-1801, doi: 10.1016/j.tet.2018.02.038.
[37] H. Tazarki, W. Zeinyeh, Y.J. Esvan, S. Knapp, D. Chatterjee, M. Schroder, A.C. Joerger, J. Khiari, B. Josselin, B. Baratte, S. Bach, S. Ruchaud, F. Anizon, F. Giraud, P. Moreau, New pyrido[3,4-g]quinazoline derivatives as CLK1 and DYRK1A inhibitors: synthesis, biological evaluation and binding mode analysis, Eur. J. Med. Chem. 166 (2019) 304-317, 10.1016/j.ejmech.2019.01.052.
[38] T. Anastassiadis, S.W. Deacon, K. Devarajan, H. Ma, J.R. Peterson, Comprehensive assay of kinase catalytic activity reveals features of kinase inhibitor selectivity, Nat. Biotechnol. 29(11) (2011) 1039-1045, 10.1038/nbt.2017.

[39] A. Jorda, M. Aldasoro, C. Aldasoro, S. Guerra-Ojeda, A. Iradi, J.M. Vila, J. Campos-Campos, S.L. Valles, Action of low doses of aspirin in inflammation and oxidative stress induced by aβ1-42 on astrocytes in primary culture, Int. J. Med. Sci. 17(6) (2020) 834-843, 10.7150/ijms.40959.
[40] H.R. Powell, T.G.G. Battye, L. Kontogiannis, O. Johnson, A.G.W. Leslie, Integrating macromolecular X-ray diffraction data with the graphical user interface iMosflm, Nat. Protoc. 12(7) (2017) 1310-1325, 10.1038/nprot.2017.037.
[41] P.R. Evans, G.N. Murshudov, How good are my data and what is the resolution?, Acta Crystallogr., Sect. D Biol. Crystallogr. 69(7) (2013) 1204-1214, 10.1107/s0907444913000061.
[42] J. Sliwiak, M. Jaskolski, Z. Dauter, A.J. McCoy, R.J. Read, Likelihood-based molecular-replacement solution for a highly pathological crystal with tetartohedral twinning and sevenfold translational noncrystallographic symmetry, Acta Crystallogr., Sect. D Biol. Crystallogr. 70(2) (2014) 471-480, 10.1107/s1399004713030319.
[43] J.A. Bertrand, S. Thieffine, A. Vulpetti, C. Cristiani, B. Valsasina, S. Knapp, H.M. Kalisz, M. Flocco, Structural Characterization of the GSK-3β Active Site Using Selective and Non-selective ATP-mimetic Inhibitors, J. Mol. Biol. 333(2) (2003) 393-407, 10.1016/j.jmb.2003.08.031.
[44] A. Casanal, B. Lohkamp, P. Emsley, Current developments in Coot for macromolecular model building of Electron Cryo-microscopy and Crystallographic Data, Protein Sci. 29(4) (2020) 1069-1078, 10.1002/pro.3791.
[45] O. Kovalevskiy, R.A. Nicholls, F. Long, A. Carlon, G.N. Murshudov, Overview of refinement procedures within REFMAC5: utilizing data from different sources, Acta Crystallogr., Sect. D Struct. Biol. 74(3) (2018) 215-227, 10.1107/s2059798318000979.
[46] S. Berg, M. Bergh, S. Hellberg, K. Högdin, Y. Lo-Alfredsson, P. Söderman, S. von Berg, T. Weigelt, M. Ormö, Y. Xue, J. Tucker, J. Neelissen, E. Jerning, Y. Nilsson, R. Bhat, Discovery of Novel Potent and Highly Selective Glycogen Synthase Kinase-3β (GSK3β) Inhibitors for Alzheimer's Disease: Design, Synthesis, and Characterization of Pyrazines, J. Med. Chem. 55(21) (2012) 9107-9119, doi: 10.1021/jm201724m.
[47] M. Varadi, S. Anyango, M. Deshpande, S. Nair, C. Natassia, G. Yordanova, D. Yuan, O. Stroe, G. Wood, A. Laydon, A. Zidek, T. Green, K. Tunyasuvunakool, S. Petersen, J. Jumper, E. Clancy, R. Green, A. Vora, M. Lutfi, M. Figurnov, A. Cowie, N. Hobbs, P. Kohli, G. Kleywegt, E. Birney, D. Hassabis, S. Velankar, AlphaFold Protein Structure Database: massively expanding the structural coverage of protein-sequence space with high-accuracy models, Nucleic Acids Res. 50(D1) (2022) D439-D444, doi: 10.1093/nar/gkab1061.
[48] Schrödinger Release 2022-2: Maestro, Schrödinger, LLC, New York, NY, 2021,
[49] Schrödinger Release 2022-2: LigPrep, Schrödinger, LLC, New York, NY, 2021,
[50] G.M. Sastry, M. Adzhigirey, T. Day, R. Annabhimoju, W. Sherman, Protein and ligand preparation: parameters, protocols, and influence on virtual screening enrichments, J. Comput. Aided Mol. Des. 27(3) (2013) 221-234, doi: 10.1007/s10822-013-9644-8.
[51] Schrödinger Release 2022-2: Protein Preparation Wizard; Epik, Schrödinger, LLC, New York, NY, 2021; Impact, Schrödinger, LLC, New York, NY; Prime, Schrödinger, LLC, New York, NY, 2021,
[52] R.A. Friesner, R.B. Murphy, M.P. Repasky, L.L. Frye, J.R. Greenwood, T.A. Halgren, P.C. Sanschagrin, D.T. Mainz, Extra Precision Glide: Docking and Scoring Incorporating a Model of Hydrophobic Enclosure for Protein-Ligand Complexes, J. Med. Chem. 49(21) (2006) 6177-6196, doi: 10.1021/jm051256o.
[53] T.A. Halgren, R.B. Murphy, R.A. Friesner, H.S. Beard, L.L. Frye, W.T. Pollard, J.L. Banks, Glide: A new approach for rapid, accurate docking and scoring. 2. Enrichment factors in database screening, J. Med. Chem. 47(7) (2004) 1750-1759, doi: 10.1021/jm030644s.
[54] R.A. Friesner, J.L. Banks, R.B. Murphy, T.A. Halgren, J.J. Klicic, D.T. Mainz, M.P. Repasky, E.H. Knoll, M. Shelley, J.K. Perry, D.E. Shaw, P. Francis, P.S. Shenkin, Glide: A new approach for rapid,

accurate docking and scoring. 1. Method and assessment of docking accuracy, J. Med. Chem. 47(7) (2004) 1739-1749, doi: 10.1021/jm0306430.
[55] Schrödinger Release 2022-2: Glide, Schrödinger, LLC, New York, NY, 2021,
[56] SZMAP 1.6.3.0: OpenEye Scientific Software, Santa Fe, NM. http://www.eyesopen.com (2013),
[57] H.E. Gottlieb, V. Kotlyar, A. Nudelman, NMR chemical shifts of common laboratory solvents as trace impurities, J. Org. Chem. 62(21) (1997) 7512-7515, doi: 10.1021/jo971176v.
[58] Q. Chen, X. Mollat du Jourdin, P. Knochel, Transition-metal-free BF3-mediated regioselective direct alkylation and arylation of functionalized pyridines using Grignard or organozinc reagents, J. Am. Chem. Soc. 135(13) (2013) 4958-4961, doi: 10.1021/ja401146v.
[59] A. Ianevski, A.K. Giri, T. Aittokallio, SynergyFinder 2.0: visual analytics of multi-drug combination synergies, Nucleic Acids Res. 48(W1) (2020) W488-W493, doi: 10.1093/nar/gkaa216.